NASA/TM-20220015470

Design of an Open Rotor, Braced-Wing Electric Transport

Jeffrey J. Berton
Glenn Research Center, Cleveland, Ohio

December 2022

NASA STI Program . . . in Profile

Since its founding, NASA has been dedicated to the advancement of aeronautics and space science. The NASA Scientific and Technical Information (STI) Program plays a key part in helping NASA maintain this important role.

The NASA STI Program operates under the auspices of the Agency Chief Information Officer. It collects, organizes, provides for archiving, and disseminates NASA's STI. The NASA STI Program provides access to the NASA Technical Report Server—Registered (NTRS Reg) and NASA Technical Report Server—Public (NTRS) thus providing one of the largest collections of aeronautical and space science STI in the world. Results are published in both non-NASA channels and by NASA in the NASA STI Report Series, which includes the following report types:

- TECHNICAL PUBLICATION. Reports of completed research or a major significant phase of research that present the results of NASA programs and include extensive data or theoretical analysis. Includes compilations of significant scientific and technical data and information deemed to be of continuing reference value. NASA counter-part of peer-reviewed formal professional papers, but has less stringent limitations on manuscript length and extent of graphic presentations.

- TECHNICAL MEMORANDUM. Scientific and technical findings that are preliminary or of specialized interest, e.g., "quick-release" reports, working papers, and bibliographies that contain minimal annotation. Does not contain extensive analysis.

- CONTRACTOR REPORT. Scientific and technical findings by NASA-sponsored contractors and grantees.

- CONFERENCE PUBLICATION. Collected papers from scientific and technical conferences, symposia, seminars, or other meetings sponsored or co-sponsored by NASA.

- SPECIAL PUBLICATION. Scientific, technical, or historical information from NASA programs, projects, and missions, often concerned with subjects having substantial public interest.

- TECHNICAL TRANSLATION. English-language translations of foreign scientific and technical material pertinent to NASA's mission.

For more information about the NASA STI program, see the following:

- Access the NASA STI program home page at http://www.sti.nasa.gov

- E-mail your question to help@sti.nasa.gov

- Fax your question to the NASA STI Information Desk at 757-864-6500

- Telephone the NASA STI Information Desk at 757-864-9658

- Write to:
  NASA STI Program
  Mail Stop 148
  NASA Langley Research Center
  Hampton, VA 23681-2199

NASA/TM-20220015470

Design of an Open Rotor, Braced-Wing Electric Transport

Jeffrey J. Berton
Glenn Research Center, Cleveland, Ohio

National Aeronautics and
Space Administration

Glenn Research Center
Cleveland, Ohio 44135

December 2022

Acknowledgments

This study was performed with support from NASA's Advanced Air Transport Technology Project of the Advance Air Vehicles Program. Special thanks go to William Haller, Jesse Quinlan, and Eric Hendricks of NASA for establishing the project's advanced concept studies, and to Mark Guynn and James Felder of NASA for reviewing this manuscript.

This report is a formal draft or working paper, intended to solicit comments and ideas from a technical peer group.

This report contains preliminary findings, subject to revision as analysis proceeds.

This work was sponsored by the Advanced Air Vehicle Program at the NASA Glenn Research Center

Level of Review: This material has been technically reviewed by technical management.

This report is available in electronic form at https://www.sti.nasa.gov/ and https://ntrs.nasa.gov/

Design of an Open Rotor, Braced-Wing Electric Transport

Jeffrey J. Berton
National Aeronautics and Space Administration
Glenn Research Center
Cleveland, Ohio 44135

Abstract

A notional, 19-passenger, battery-powered, fully electric airplane is investigated in this study. It is designed to serve the regional aviation market of the near future. Three strategies are used to reduce energy demands placed on its batteries: 1) a high aspect ratio, braced wing, 2) two efficient open rotor propellers, and 3) flying at comparatively low cruise speeds. It has an otherwise conventional airframe architecture. Parametric system weight, aerodynamic, propeller, and mission performance models are developed. Single-rotation and contra-rotation propellers are studied. Implementation of a novel selective noise reduction system is also investigated. During sizing and optimization of its design variables, battery cell specific energy is treated as a technology parameter that is varied to determine its influence on mission range. To achieve a minimum range success criterion of 250 nmi with reserves, it is found that battery cell specific energy must be at least 600 W-h/kg, more than twice the capability of today's lithium-ion cells.

1.0 Introduction

Electric airplanes are potentially disruptive innovations enabled by rapidly emerging battery and electronic technologies. Better airplanes are promised by clever, synergistic integration of electric propulsion with airframe structures and control systems. Concepts could be either entirely electric or electrical hybrids. Transformative new airplane architectures may be possible by exploiting "distributed electric propulsion" (e.g., Refs. 1 to 4).

But, if battery technologies arrive sooner than transformative aircraft technologies (or if transformative aircraft technologies fail to emerge or become popular), then it is possible that electric airplanes will have more conventional architectures. In the near term, at least, advanced electric airplanes could appear with otherwise ordinary-looking features. This study is an attempt to define an airplane in this scenario, and to determine roughly the battery characteristics needed to support it.

Although battery technology is progressing quickly, researchers usually cite battery performance as the most significant barrier to the viability of fully electric aircraft. In particular, most studies identify shortfalls in battery cell specific energy. Some vehicle concepts require specific energies well beyond the capability of today's lithium-ion cells, with the problem becoming more severe as payload or range requirements increase (e.g., Refs. 5 to 11).

Thus, it is of interest to see if a small, fully electric transport can be made viable when the demands placed on its batteries are reduced. Three strategies that reduce energy requirements are considered. Improving propulsive efficiency, improving vehicle aerodynamics, and optimizing cruising airspeed are all effective means of reducing energy requirements.

Cruising relatively slowly (if it is acceptable to do so) directly reduces power requirements, and it can result in less energy to fly a mission by cruising closer to a maximum lift-to-drag ratio condition. High levels of propulsive efficiency can be achieved with efficient, open rotor propellers. Contra-rotation propellers that convert swirl losses into useful forward thrust are investigated. Electric motors may

improve the implementation prospects of contra-rotation simply by being more compact than gas turbine engines. Wings with large spans have very low lift-dependent drag. A classic means of enabling high wingspan is through use of a wing brace. The brace relieves the bending moment at the wing root and enables high-span designs without the weight penalty that would result from a cantilever design. Using a wing brace for this concept capitalizes on the rekindled interest in braced wings (Ref. 12), though at a much lower airspeed than other braced concepts under investigation (e.g., Ref. 13).

Mission energy per passenger-mile is often used as a measure of merit in aircraft design. Maximizing the number of passengers allowed by type category regulations is hypothesized to minimize this metric. The highest number of passengers permitted by U.S. FAA Part 23 (Ref. 14) and by European CS-23 (Ref. 15) regulations for normal-category airplanes is 19. So to state the problem formally, the goal of this study is to determine the minimum battery specific energy required to enable a 19-passenger commuter transport while using airframe technologies that might be available by about 2035. Alternative designs having fewer passengers is investigated as a sensitivity in a later section.

The Open Rotor, Braced-Wing Electric Transport studied here is dubbed "ORBET." Though it is fully electric (and is therefore advanced in many ways), it is otherwise conventional and uses relatively near-term technologies wherever possible. For example, ORBET does not rely on distributed propellers to enhance lift via a "blown wing" effect, nor does it relocate its propellers to the wing tips to recover vortex energy. In other words, ORBET is not intended to be a larger version of NASA's experimental X-57 Maxwell (Ref. 1). ORBET does not rely on superconductor materials (high-temperature or otherwise) to reduce electrical system losses and weight, and it does not rely on boundary-layer ingestion to reduce drag, as is proposed for other futuristic electric airplane concepts (e.g., Refs. 2 and 16). The lack of advanced features results in an otherwise conventional appearance.

ORBET is proposed to serve the so-called "Regional Air Mobility" (RAM) aviation market of the future. Although a common nomenclature has yet to emerge, RAM refers usually to low-demand routes characterized by shorter distances. They differ from the transcontinental or intercontinental trunk routes serviced by large-capacity airplanes involving at least one large airport, and they also differ from the regional or interregional routes serviced by smaller jets and turboprops. The RAM market consists of short, intraregional connections and point-to-point service between airports in urban, suburban, or rural areas. Service can be scheduled or on-demand, and payloads can be either passengers or freight. RAM service has also been referred to as "thin-haul" aviation, since the frequency of flights for any individual route is low, or "thin."

The need for a RAM transportation system that is separate – to the extent possible – from the long-haul system was recognized as early as 1971 (Ref. 17). Today, RAM routes are served by small-capacity airplanes carrying typically 7 to 19 passengers or small cargo loads. Their airworthiness directives are given in the U.S. by (Ref. 14) and in Europe by (Ref. 15). RAM airplanes are often multi-role utility transports that target the commuter or VIP passenger market, small package delivery, and mail delivery. RAM operations are a subset of what NASA refers to more broadly as Advanced Air Mobility missions that are characterized by routes of 300 nmi or less (Ref. 18). Mostly, these routes have been abandoned by high-volume commercial operators because their larger aircraft are costlier to operate with reduced payloads. RAM routes are served usually by boutique commuter operators using smaller equipment.

It can be challenging for RAM services to operate profitably. Operating costs per available seat mile for RAM carriers are more than three times higher than for large air carriers (Ref. 19). And RAM operators must compete with surface modes of travel such as automobiles, buses, trucks, and rail. This is true especially within densely traveled corridors, where customers have multiple mode and schedule choices. Still, though the frequency of flights for any individual route is low, the cumulative number of flights across the entire RAM network is significant. And in the U.S., the economics of RAM aviation are

improved for some routes via subsidies paid to operators by the Essential Air Service program (Ref. 20). The RAM market is undergoing change. The growth in pushbutton e-commerce and the oversubscribed (for now, at least) shipping network have created opportunities for RAM aviation. The recently certificated Cessna 408 SkyCourier (Ref. 21), developed primarily for launch customer FedEx, is expected to serve RAM freight markets where larger airplanes cannot operate competitively. A passenger variant of the SkyCourier is the first entirely new 19-passenger airplane in decades. In the future, the dense (and underused) network of airfields covering the U.S. and Europe could be better exploited. Of the roughly 4900 operational public airports in the U.S. today, only 11 percent of them have commercial operations (Ref. 22). Many of the remaining airports have surplus capacity that could be used to enhance RAM economics. Studies (e.g., Refs. 23 and 24) have determined that future hybrid-electric RAM airplanes can be operated profitably.

Despite the advantages that technologies may bring, fully electric aircraft are nevertheless likely to be handicapped by the comparatively low specific energy of their batteries relative to liquid fuels. Kerosene-based fuels have more than a 40-fold specific energy advantage compared to today's lithium-ion batteries. Even when the efficiencies of converting energy to useful mechanical work are considered, fuel-burning engines still have a clear specific energy advantage over today's batteries. It is anticipated that, at least for the foreseeable future, fully electric aircraft will have a distinct disadvantage in range capability under comparable conditions to fuel-burning aircraft such as the SkyCourier (Ref. 25). But, there is increasing environmental awareness of carbon production. In the future, there may be a need for more sustainable aircraft concepts like ORBET. Operators might relax airplane performance requirements (especially maximum range capability), particularly if there are incentives or requirements to do so. Though some operators might have a genuine, occasional need for long-range capability, missions flown in RAM aviation are almost always far shorter than the maximum range capabilities of the aircraft that service them (e.g., Ref. 26). On future RAM routes, such as those from Tucson to Tucumcari, or from Tehachapi to Tonopah, operators might be served adequately well by fully electric transports having shorter range than today's fuel-burning transports.

This is an initial airplane design and concept feasibility study conducted as a part-time effort over nine months during 2021. Due to the short time involved, this study does not assess the concept's economic prospects, its operating costs, or the additional airport infrastructure required to support it. Electrical components and power management systems are not designed or analyzed in detail (NASA already has research ongoing in these areas, e.g., Reference 27). Instead, electrical components are treated as simple systems, with their performance and weight modeled by simple efficiency assumptions and scalar models. This study is intended to broadly define a near-term, fully electric, 19-passenger concept airplane and determine its battery specific energy requirements. Future work is needed to model the concept and its economics more rigorously.

2.0 Design

ORBET has seating for up to 19 passengers and flies at airspeeds no greater than 250 kcas.[1] With regards to type classification (see section 2005 of References 14 and 15), it is an airplane in the "normal" category, it has a "level 4" certification classification (with maximum seating varying between 10 and 19 passengers), and it is in the "low-speed" performance category. Airplanes of this type were formerly in the so-called commuter category, but that term is deprecated following the restructuring and

[1]Throughout this document, abbreviations for calibrated airspeed and true airspeed (in knots) are expressed as kcas and ktas, respectively.

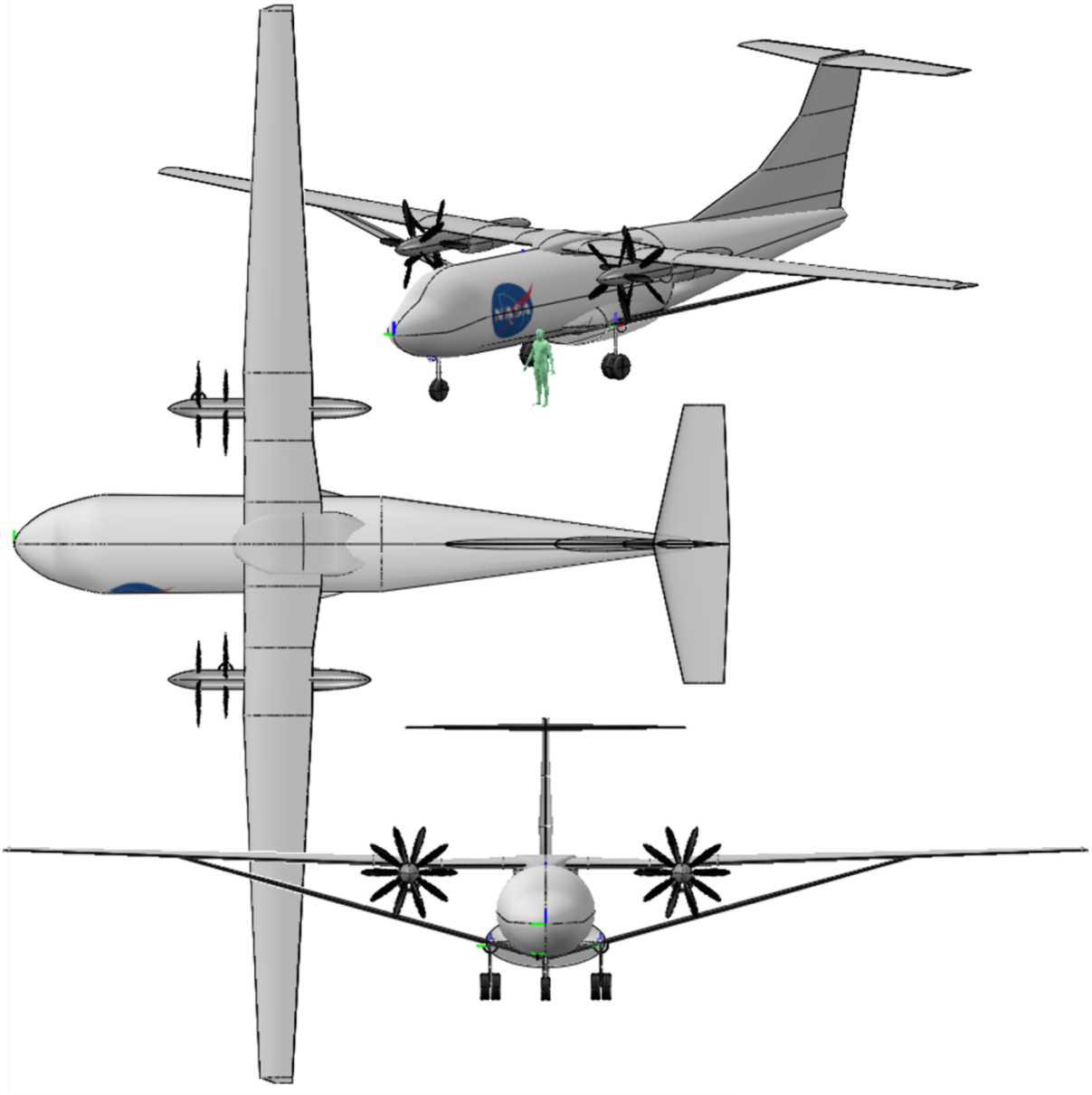

Figure 1.—Solid model of the ORBET concept.

harmonization of regulations in the U.S. and in Europe in 2017. A solid model of ORBET is shown in Figure 1. The variant having contra-rotation propellers is shown.

2.1 Performance Requirements

Performance requirements must be defined for ORBET so that it can be sized and optimized, and so that the minimum battery specific energy can be determined. Chief among the requirements are targets for mission range and takeoff and landing field distance, which are driven principally by market and route demands. A statement of all performance requirements is given later in Section 7.0.

Most often, mode of travel statistics, economic studies, and existing air routes are used to provide insight into setting a range requirement for an airplane in this class. For shorter trips, there is usually a breakpoint in trip distance where surface modes fall off and where air travel modes begin. Sources place this breakpoint variably from 100 to 500 statute miles (87 to 434 nmi; (e.g., Refs. 28 and 29)). Economic studies indicate that markets exist in the U.S. and in Europe to support a 19-passenger transport to serve regional air mobility markets with ranges of 100 to 500 km (54 to 270 nmi; (e.g., Ref. 30)). And in 2016, Cape Air (the largest commuter airline in the United States) reported that 67 percent of their routes are shorter than 100 nmi, and all of their routes are shorter than 225 nmi (Ref. 26).

Energy to fly an additional reserve mission is also required. Operators of today's fuel-burning airplanes must comply with reserve requirements defined in section 167 of Reference 31. It is anticipated that operators of electric airplanes will need to satisfy similar requirements. Therefore, ORBET is required to have enough battery energy to cruise an additional 45 min at normal airspeed following completion of the primary flight to its intended airport. The diversion allotment required for fuel-burning airplanes in section 167(a)(2) of Reference 31 is assumed not to apply (with adequate ceiling and visibility conditions, at least) since ORBET could be designed with equipment for an instrument approach.

Given these considerations, ORBET is assigned a minimum range success criterion of 250 nmi, with additional reserve energy for 45 min of flight at optimum speed and altitude. Minimum battery specific energy is determined from this criterion. The design mission is shown in Figure 2. Cruise airspeed and cruise altitude are design variables subject to optimization. Reserves are modeled as a simple 45-min hold at 8000 ft.

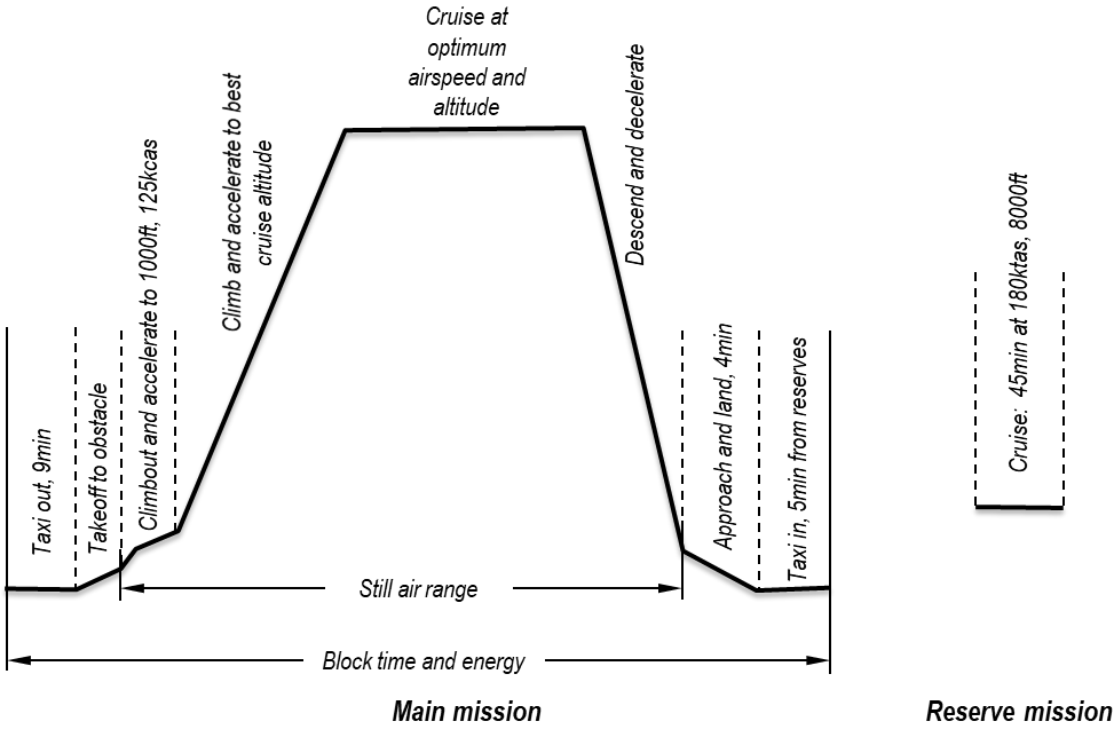

Figure 2.—Design mission profile.

Small airfields must be accessible to RAM transports. An airplane's takeoff and landing distances are often used as surrogate indicators for airport accessibility. A maximum field distance appropriate for ORBET must be defined. It should not be so large that operations to smaller airfields are constrained. In the U.S., 96 percent of the population lives within 19 miles of an airport having a runway at least 4000 ft long (Ref. 32): a distance that can be driven easily in a car, taxi, or a rideshare service. Of the nearly 4900 operational public airports in the U.S. today, more than half of them have runways 4000 ft in length or longer (Ref. 22). Given these considerations, ORBET is constrained to takeoff and landing distances no greater than 4000 ft.

Many sources fail to define precisely what is meant by takeoff field distance. Larger multiengine airplanes like ORBET require a critical field distance calculation with one engine inoperative (see section 2115(c) of Reference 14). This is sometimes referred to as a balanced field length calculation. In this study, the critical field distance to a 35 ft runway obstacle from a flat, paved, dry, sea level field at 59 °F is evaluated. Takeoffs are evaluated at maximum gross weight and at maximum motor power. An ordinary takeoff at 59 °F with both engines operating is also computed. In normal situations when both engines are operating, the required field distance is much shorter. This type of takeoff is used to compute reference profiles for noise certification (see section 9.0 and Chapter 10 of ICAO noise regulations (Ref. 33)). NASA's Flight Optimization System (FLOPS, Ref. 34) is used to compute both takeoff types. A discussion of how critical field distance is calculated for Part 23 airplanes using FLOPS is given in Section 6.0.

2.2 Description

ORBET has a layout, gross weight, payload, shaft power, and airspeed similar to the new SkyCourier turboprop (Ref. 21), and it is somewhat similar to other 19-passenger turboprops with braced wings and unpressurized cabins (Refs. 35 to 37). But it is thought that ORBET's wing aspect ratio could be much higher than any of these examples, since it is intended to leverage new research into braced-wing technology (e.g., Refs. 38 to 43).

ORBET is proposed to have a maximum takeoff gross weight of 18,000 lb. This is nearly the 19,000 lb upper limit for Part 23 commuter transports. For high propulsive efficiency, ORBET has large-diameter propellers, necessitating a high-set wing and wing-mounted powerplants. Its wing is braced with streamlined struts. ORBET's wing may be stiffer and less elastic than larger braced-wing concepts (e.g., Ref. 13), so it is assumed that additional jury structural members are unnecessary. If true, then interference drags and supervelocity flow between structures (i.e., flow at velocities higher than freestream velocity) should be similar to other braced-wing airplanes. Unlike other electric concepts that exploit distributed electric propulsion, ORBET's wing is not sized for cruise conditions. Instead, it has a necessarily larger wing that results in good climb performance and short field distance. Despite a large wing, its low cruise airspeed enables ORBET to cruise near its maximum lift-to-drag ratio condition. Wing size, aspect ratio, and propeller diameter are determined during the sizing and optimization process described in Section 7.0.

Two electric motor powerplants are podded on the wing in a traditional tractor configuration. There are advantages and disadvantages to tractor arrangements. They have downstream blockage losses, and they could disturb any natural laminar flow on the wing that might otherwise be present. But compared to pusher configurations, tractor propellers enjoy smoother incoming freestream flow, and they lack additional noise generated by impinging wing wakes. A pusher variant of ORBET is not analyzed.

ORBET's unpressurized cabin has two pilots on a flight deck and has accommodations for up to 19 passengers seated three abreast (or optional equivalent freight). All structure makes maximum use of advanced materials and composites wherever possible. The main landing gear is retractable into fuselage

blister fairings. The nose gear folds forward into the fuselage. Single-slotted extensible (Fowler) trailing edge flaps are interrupted by the nacelles. There are no leading edge high-lift devices. Actuators for all systems are proposed to be operated by conventional hydraulics. Cruise is limited to a maximum altitude of 10,000 ft, a popular cruising altitude for unpressurized aircraft with no supplemental oxygen (see section 211 of Reference 31).

Stability and control of ORBET is not explicitly studied. Instead, a simple volume coefficient method is used to size its horizontal and vertical tails. A modified tail volume sizing method is available in NASA's FLOPS code (Ref. 44). This method is used to size ORBET's tails, since FLOPS is used also for other tasks (as discussed in later sections). Regression correlations for horizontal and vertical tail volume coefficients are based on historical aircraft data. It should be noted that the FLOPS regressions fail at the limit for wings having zero sweep. When wing sweep nears zero (as in the case of ORBET), the correlations for horizontal and vertical tail volume coefficients tend to infinity and to zero, respectively. This is remedied in this study by specifying a quarter-chord wing sweep of 25° (i.e., the lowest quarter-chord sweep considered in the FLOPS historical data) and using the resulting volume coefficients values.

All power management electronics are proposed to reside in the wing nacelles. The power management system is conventional (i.e., not superconducting) and is cooled by air taken in via scoop inlets on the underside of each nacelle. Batteries are proposed to lie under the cabin floor. There are two packs: a larger pack is located forward of the main landing gear; a smaller pack is to the rear. They could be removed from below with simple equipment; perhaps even during quick turnarounds if it could be managed quickly enough. The volume available for batteries is estimated to be 150 ft^3.

2.3 Variants

Two variants of ORBET are studied. The first is equipped with conventional single-rotation propellers (Figure 3, left), while the second has contra-rotation propellers (Figure 3, right). The contra-rotation propellers are expected to have greater efficiency due to swirl loss reduction. This performance benefit, however, is offset by additional weight. Performance benefits of each variant are discussed in Section 8.0.

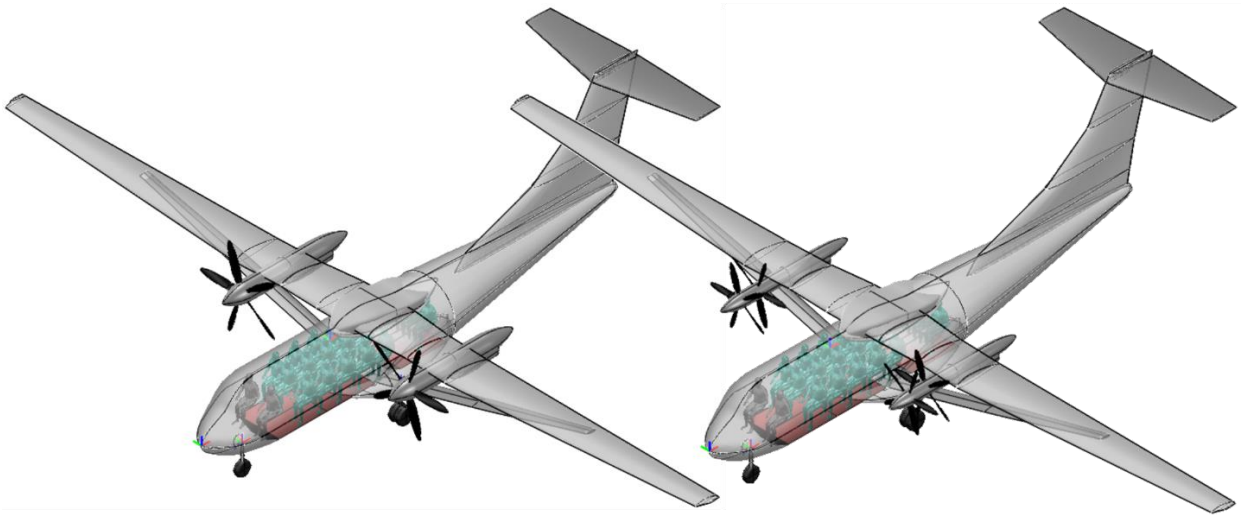

Figure 3.—ORBET variants: single-rotation propellers (left), contra-rotation propellers (right).

Because a single-rotation propeller is easier to analyze than a contra-rotation propeller, the single-rotation propeller variant is studied first. Sizing and optimization are performed using a simpler set of design variables that are appropriate for a single-rotation propeller system.

The contra-rotation propeller variant is assessed afterwards using the same airframe design as the single-rotation propeller variant. Borrowing vernacular from the aviation industry, it can be viewed as a "new engine option" variant of the initial airplane. The contra-rotation propeller analysis is described in greater detail in Sections 5.0 and 8.0.

2.4 Clarification on Use of Terminology

ORBET is described as having "open rotor" propellers. A clarification is needed. The implication of this terminology is that ORBET will benefit from nontraditional, highly efficient, contra-rotating propellers with many, thin, highly swept, wide-chord, and often scimitar-shaped blades. But if implemented as such, ORBET might have safety and certification concerns. As typically envisioned, an open rotor propeller would have many blades consisting of relatively thin airfoil sections, with each blade attached to a pitch-change mechanism in a rotor hub. In this sense, an open rotor engine is more akin to an "unducted" turbofan than a traditional propeller engine (indeed, the GE36 demonstrator engine in the 1980s was named the Unducted Fan, or UDF (Ref. 45)). As usually proposed, a thin composite blade is bonded to a metallic inner spar, which is secured to a pitch-change mechanism in the hub. The entire assembly must be able to withstand maximum centrifugal loads. A system having these features is sometimes called a "prime reliant" system (Ref. 46). But with many blade shanks crowding the hub, and with each blade requiring the ability to change pitch, it may prove difficult to design an adequate, prime reliant blade retention system for open rotors. For airplanes larger than ORBET, some of the regulations regarding this issue fall under section 25.905(d) of Reference 47 and its associated advisory (Ref. 48). For these large transports, hazards must be minimized if a propeller blade fails or if a blade is released by a hub failure. Ensuring that an open rotor propeller is prime reliant might make the engine prohibitively heavy. Smaller airplanes like ORBET have no equivalent requirement, but compliance with propeller airworthiness regulations (Ref. 49) must be demonstrated. In any case, how future open rotors might satisfy these requirements is unclear.

But the scimitar shape of open rotor propellers is driven by the need for high airspeed. ORBET's range performance, as will be shown later, benefits greatly from low-speed flight. Indeed, at ORBET's normal economy cruise speed of just 180 ktas, scimitar-shaped open rotor blades are not warranted. It should be apparent from the figures above that ORBET is equipped with quite ordinary propellers. As such, any conventional propeller installation for ORBET (with fewer, thicker, straight blades) should have plenty of room in the hub to incorporate an adequate blade retention system and to satisfy ordinary propeller requirements (Ref. 49).

3.0 Weight Model

ORBET weights are predicted using a component buildup process. Major structural and system component weights are predicted using the statistical-empirical weight relations of FLOPS (Ref. 44) and Torenbeek (Ref. 50). An original model for propeller weight is developed. In general, the relations given by Torenbeek can be applied to smaller, Part 23 normal category transports (Ref. 14) as well as to larger, Part 25 transport category transports (Ref. 47). The relations given in FLOPS, however, are most often limited to Part 25 transports. Since methods have been developed in FLOPS for high aspect ratio, strut-braced wings, and since FLOPS is used also to evaluate mission performance, the weight relations from FLOPS are used for ORBET wherever they are applicable. Torenbeek's relations, however, are used in

cases where those in FLOPS are deemed inappropriate for small transports. All of these instances are noted below. Since the relations in FLOPS are generally derived from older airplane data, scalars are frequently applied to component weights to reflect use of advanced materials and technologies. These instances are also noted. Methods for computing the weights of relevant structures and systems are detailed in the following sections. Note that ORBET is assumed to have battery and electrical system redundancies that would make an onboard auxiliary power unit unnecessary.

As noted in Section 2.0, ORBET's maximum gross weight is 18,000 lb. That is, it is set deliberately to be near the 19,000 lb upper limit for Part 23 transports. The components of its empty weight are predicted individually. Since the weight of payload and operating items are known, the weight of batteries is set by the available weight remaining. Since ORBET's mission range is dependent on the total energy contained in the batteries, an accurate weight buildup of structural components and systems is important.

Several of the statistical-empirical weight relations used in this study are dependent upon the maximum takeoff gross weight, W_{mto}. ORBET's 18,000 lb maximum gross weight, however, is unusually heavy for an airplane in its passenger class due to its batteries. Thus, if 18,000 lb were used in empirical equations containing W_{mto}, some of the resulting component weights might be unrealistically high. The weight relations for furnishings and equipment, for example, fall into this category. Instead, a weight of 12,500 lb is sometimes substituted for W_{mto}. 12,500 lb is the maximum gross weight of a 19-passenger De Havilland DHC-6-300 Twin Otter which is somewhat in the same competitive class as ORBET. Those instances are noted below.

3.1 Wing

The method built into FLOPS for estimating wing weight (Ref. 44) departs somewhat from the usual statistical-empirical approach used for other structural components. There are insufficient statistical data available to determine empirically the effects of high aspect ratio, low sweep angle, strut bracing, flutter, and aeroelastic tailoring on the weight of advanced wings. To help determine empirically the influence of these effects, optimum wing designs were developed using the Aeroelastic Tailoring and Structural Optimization program (Ref. 51). The resulting trends, some of which are shown in Reference 34, were used to develop the FLOPS wing weight estimation method. The relations are too lengthy to reproduce here. Interested readers are referred to Reference 44 for a full explanation. This method is applicable to advanced, braced-wing concepts such as ORBET. The maximum benefit of wing strut bracing, maximum use of composites, and maximum use of aeroelastic tailoring are assumed for ORBET. The wing weight estimate reacts automatically to changes in design variables during sizing and optimization (see Section 7.0).

3.2 Fuselage

The fuselage structural weight, W_{fuse}, is computed using the weight relation in FLOPS (Ref. 44):

$$W_{fuse} = 1.35 C_{fuse} \left[L_{fuse} D_{fuse} \right]^{1.28}$$

The equation from Reference 44 reduces to the above form for passenger-carrying airplanes with wing-mounted engines. L_{fuse} is the overall fuselage length in feet, and D_{fuse} is the average fuselage diameter in feet. W_{fuse} is given in pounds. L_{fuse} and D_{fuse} are obtained from the solid model of the vehicle. C_{fuse} is a technology scale factor. The overall fuselage weight is reduced by 18 percent to reflect maximum use of composites as suggested by Reference 52, and it is reduced further by 8 percent to reflect an unpressurized cabin as suggested by Reference 50. Thus, C_{fuse} is equal to 0.74.

3.3 Landing Gear

The main and nose landing gear weights, W_{main} and W_{nose}, respectively, are computed using the weight relations in FLOPS for retractable gear (Ref. 44):

$$W_{main} = 0.00995 C_{ldg} W_{ldg}^{0.95} L_{main}^{0.43}$$
$$W_{nose} = 0.04080 C_{ldg} W_{ldg}^{0.67} L_{nose}^{0.43}$$

The equations from Reference 44 reduce to the above form for transport-category airplanes. L_{main} and L_{nose} are the lengths of the extended main and nose landing gear oleos in inches, respectively, and W_{ldg} is the airplane design landing weight in pounds. W_{main} and W_{nose} are given in pounds. L_{main} and L_{nose} are obtained from the solid model of the vehicle. C_{ldg} is a technology scale factor. The gear weight is reduced by 15 percent to reflect maximum use of advanced materials as suggested by Reference 52. Thus, C_{ldg} is equal to 0.85.

Since ORBET is an all-electric transport that burns no fuel, its weight for any given mission never changes. Thus its design landing weight must equal its design maximum takeoff weight. The landing gear must be designed to bear the full 18,000 lb maximum takeoff weight upon landing. For FLOPS calculations, this is achieved by setting the ratio of maximum landing weight to maximum takeoff weight to unity.

3.4 Furnishings and Equipment

Since FLOPS is primarily a tool for Part 25 transport-category large airplanes, its weight predictions for furnishings and equipment may be too heavy if applied small Part 23 transports. Its statistical-empirical weight relation for these items presumably accounts for galley and water equipment, lavatories, insulation, non-removable emergency oxygen, evacuation slides, cargo provisions, and soundproofing, which are much lighter on (or are entirely absent from) Part 23 transports. Torenbeek (Ref. 50), however, provides relations for Part 23 category transports.

Weight relations for flight deck accommodations (W_{fda}), passenger seating (W_{seat}), fire-detection and extinguishing systems (W_{fire}), cabin floor coverings (W_{fc}), and miscellaneous cabin equipment (W_{misc}) are:

$$W_{fda} = 16 W_{dwe}^{0.285}$$
$$W_{seat} = 14 N_{pax}$$
$$W_{fire} = 0.006 W_{mto}$$
$$W_{fc} = 0.135 S_{floor}^{1.15}$$
$$W_{misc} = 0.14 V_{cabin}^{1.14}$$

All weights are in pounds. Delivery weight empty (W_{dwe}) is 7100 lb, the portion of the empty weight accounting for structural weight, propulsion, and aircraft systems, but not batteries, furnishings, or interior equipment. N_{pax} is the maximum number of passengers. W_{mto} is the maximum takeoff gross weight in pounds (taken as 12,500 lb as explained above). S_{floor} and V_{cabin} are the passenger cabin floor area in square feet and volume in cubic feet, taken from the ORBET solid model.

3.5 Anti-Ice System

Since FLOPS is primarily a tool for transport-category large airplanes, its weight relation for anti-ice systems is based on engine customer bleed air. For an all-electric transport like ORBET, an electrically heated system might be more simply implemented than a bleed-fed system. And unlike the electrically heated systems that are currently available, a dedicated alternator would not be necessary. Scaling the

information from Reference 53 to the size of ORBET (and considering only the resistance-heat foils), the anti-ice system for ORBET is estimated to weigh a constant 50 lb in all cases. When evaluating mission performance, the anti-ice system is assumed to be turned off.

3.6 Avionics and Instruments

The FLOPS relation for avionics weight is a function of design range, which may not be appropriate for a short-range, RAM transport like ORBET. Torenbeek (Ref. 50), however, provides a relation for avionics and instruments weight, W_{inst}, for Part 23 low-speed transports operating under instrument flight rules:

$$W_{inst} = 120 + 20N_W + 0.006W_{mto}$$

N_W is the number of wing-mounted engines and W_{mto} is the maximum takeoff gross weight in pounds (taken as 12,500 lb as explained above). W_{inst} is given in pounds.

3.7 Hydraulic Systems

The hydraulic system weight, W_{hyd}, is computed using the weight relation in FLOPS (Ref. 44):

$$W_{hyd} = 0.57C_{hyd}(A_{fuse} + 0.27S)(1 + 0.3N_W)(3000/P_{hyd})^{0.35}M_{max}^{0.33}$$

The equation from Reference 44 reduces to the above form for fixed-wing airplanes with wing-mounted engines. The relation assumes control surfaces are actuated by a conventional, fully duplicated hydraulic and pneumatic system operating at 3000 psi. A_{fuse} is the overall fuselage planform area in square feet, S is the reference wing area in square feet, N_w is the number of wing-mounted engines, P_{hyd} is the hydraulic system pressure in psi, M_{max} is the maximum operating Mach number, and C_{hyd} is a technology scale factor. Weight is reduced by 15 percent to reflect an advanced system. Thus, C_{hyd} is 0.85. W_{hyd} given in pounds.

3.8 Surface Controls

The weight of surface controls, W_{sc}, is computed using the weight relation in FLOPS (Ref. 44):

$$W_{sc} = 1.1C_{sc}M_{max}^{0.52}S_{flap}^{0.6}W_{mto}^{0.32}$$

Where M_{max} is the maximum operating Mach number, S_{flap} is the total movable wing surface area in square feet, C_{sc} is a technology scale factor, and W_{mto} is the maximum takeoff gross weight in pounds (taken as 12,500 lb as explained above). Weight is reduced by 15 percent to reflect use of advanced materials as suggested by Reference 52. Thus, C_{sc} is 0.85. W_{sc} is given in pounds.

3.9 Tail

Weights of the horizontal tail (W_{HT}) and the vertical tail (W_{VT}) are computed using the weight relations in FLOPS (Ref. 44):

$$W_{HT} = 0.53C_{HT}S_{HT}W_{mto}^{0.2}(\lambda_{HT} + 0.5)$$
$$W_{VT} = 0.32C_{VT}S_{VT}^{0.85}W_{mto}^{0.3}(\lambda_{VT} + 0.5)$$

The equations from Reference 44 reduce to the above form for single-tail airplanes. The subscripts refer to the horizontal tail and the vertical tail. S_{HT} and S_{VT} are the theoretical tail areas in square feet, determined by the modified volume coefficient method described in Section 2.0. λ_{HT} and λ_{VT} are the theoretical taper ratios. C_{HT} and C_{VT} are technology scale factors. W_{mto} is the maximum takeoff gross weight in pounds (taken as 12,500 lb as explained above). Weights are reduced by 25 percent to reflect

use of advanced composite materials as suggested by Reference 52. Thus, C_{HT} and C_{VT} are equal to 0.75. W_{HT} and W_{VT} are given in pounds.

3.10 Nacelles

The weight of one nacelle, W_{nac}, is computed using the weight relation in FLOPS (Ref. 44):

$$W_{nac} = 0.25 C_{nac} D_{nac} L_{nac} F_{SLS}^{0.36}$$

Where D_{nac} is the average nacelle diameter in feet, L_{nac} is the length of a nacelle in feet, C_{nac} is a technology scale factor, and F_{SLS} is the rated thrust of one powerplant at the sea level static condition in pounds. Weight is reduced by 20 percent to reflect use of advanced composite materials as suggested by Reference 52. Thus, C_{nac} is 0.80. W_{nac} is given in pounds.

3.11 Propellers

FLOPS (Ref. 44) has no propeller weight model. Roland (Ref. 54) proposed a correlation in 1969, but it is regressed against older propeller data that spans a rather wide range of applications. An improvement to Roland's correlation is sought that uses newer propeller weight data for a narrower regression space that is more applicable to ORBET. Roland's independent correlating variable, $DP_{max}\sqrt{B}$, is retained, where D is the propeller diameter in feet, P_{max} is the maximum rated takeoff shaft power in bhp, and B is the number of blades.

For the new correlation, emphasis is placed on propellers newer than those considered by Roland, and propellers having very large values of $DP_{max}\sqrt{B}$ (such as Dowty's R408/6-123-F and R381/6-123-F/5 models found on the Bombardier Q400 and the Saab 2000), are excluded. Data for fifty variable-pitch, hydraulically operated propellers with feathering and reversing features manufactured by Hartzell Propeller, Collins Aerospace, Dowty Propellers, and MT-Propeller are taken from their Type Certificate Datasheets. Both aluminum and composite construction is considered.

The resulting new correlation for the weight of a single propeller, W_{prop}, is:

$$W_{prop} = 1.936\left(DP_{max}B^{0.5}\right)^{0.4423}$$

W_{prop} accounts for the weight of the propeller blades, hub, pitch-change mechanism, and spinner. W_{prop} is given in pounds. The original and revised correlation are plotted with data in Figure 4. The propeller weight of the final, optimized single-rotation variant of ORBET is shown on the plot. The revised correlation results in lighter weight predictions than Roland's 1969 model.

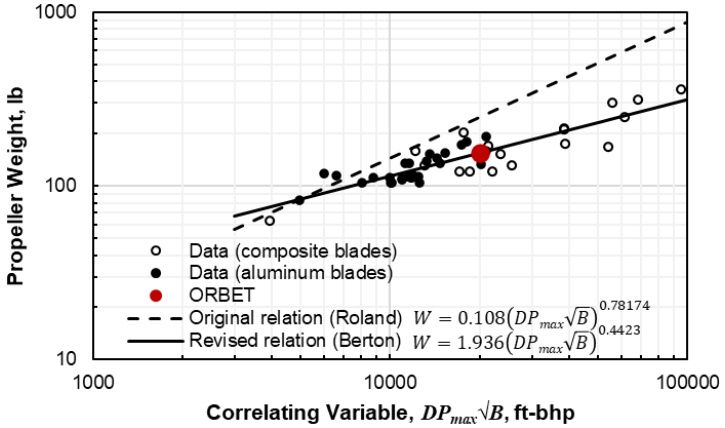

Figure 4.—Propeller weight model.

3.12 Electric Motors and Power Conditioning Equipment

The weight of an electric motor powerplant, W_{motor}, and its associated power management and distribution equipment, W_{PMAD}, are estimated using two simple linear scalar models:

$$W_{motor} = 0.164 P_{max}$$

$$W_{PMAD} = 0.0822 P_{max} + 200$$

The power, P_{max}, is the maximum rated power of a single powerplant contained within a single nacelle installation. For example, a P_{max} of 1000 bhp would power the propeller on one side of the airplane during takeoff, whether it is a single-rotation propeller or a set of two contra-rotation propellers each using some portion of that power. Further complicating this accounting is that there may be more than one electric motor per powerplant totaling 1000 bhp. That is, two electric motors per nacelle might be employed for motor efficiency considerations, where one motor could be disengaged from the shaft during cruise when less shaft power is required.

So to clarify, in this example for P_{max} equaling 1000 bhp, all of the electric motors on the airplane would weigh a total of (0.164 lb/bhp)(1000 bhp)(2) = 328 lb, all of the associated power conditioning electronics would weigh a total of (0.0822 lb/bhp)(1000 bhp)(2) + (200 lb)(2) = 564 lb, and the total power consumed by the airplane during the takeoff maximum would be (1000 bhp)(2) = 2000 bhp.

P_{max} is a design variable determined by the sizing and optimization process (see Section 7.0). The power management system is conventional, i.e., not superconducting. The coefficients in the equations are based on high specific power electric motors under development for aviation applications (e.g., Refs. 55 and 56). Note that 0.164 lb/bhp and 0.0822 lb/bhp equate to specific power levels of 10 kW/kg and 20 kW/kg, respectively. The 200 lb adder used in the W_{PMAD} relation is intended to account for the traditional electrical equipment required for conventional airplanes. W_{motor} and W_{PMAD} are given in pounds.

3.13 Flight Crew and Payload

The weight of two crew members with their baggage and flight equipment is assumed. Although some futuristic studies assume that increases in automation may someday enable single-pilot operations, current requirements for flight crews require a captain and a second in command. Specifically, 14 CFR§135.99(b) (Ref. 57) states “No certificate holder may operate an aircraft without a second in command if that aircraft has a passenger seating configuration, excluding any pilot seat, of ten seats or more.” Single-pilot operation without a second in command is investigated as a sensitivity in a later section. Torenbeek (Ref. 50) suggests using 205 lb per pilot with their baggage and flight equipment. The weight per passenger assumed is 170 lb. Baggage is assumed to weigh 30 lb per passenger. Payload for a 19-passenger mission thus weighs 3800 lb. Operating items (i.e., the flight crew and their baggage) weigh 410 lb.

3.14 Batteries, Power, and Iteration to Closure

The weight of batteries is what remains after subtracting the weights of structural components, systems, payload, and operating items (each described above) from the 18,000 lb maximum takeoff gross weight. This accounting is similar to how fuel weight is sometimes determined during conceptual design of conventional fuel-burning aircraft. Several of ORBET’s design variables (see Section 7.0) influence the component weights listed above. Thus, the weight models must react properly to changes in design

variables during the optimization and sizing process. This requires an iteration to determine the final weight of each component and the weight available for batteries.

4.0 Aerodynamic Model

4.1 Analysis Method

An aerodynamic model with relatively low computational cost is required to provide vehicle aerodynamics to the sizing and optimization process described in Section 7.0. Given airfoil section performance and a basic vehicle definition, the model must be able to compute airplane lift and drag coefficients as functions of its angle of attack. It must react to changes in gross airplane geometry so that airplane-related design variables can be optimized. It must provide both clean aerodynamics and flapped aerodynamics suitable for takeoff and landing analyses.

A semiempirical method developed by Roskam (Ref. 58) is selected and programmed so that it can be executed by a driver during sizing and optimization. Modeling begins by selecting two-dimensional airfoil sections for the wing with known sectional lift and drag properties. Lift and drag coefficients of the airfoil sections are represented in the model by simplified characterization parameters (i.e., primitives), rather than by continuously real functions. These primitives (such as the lift-curve slope, maximum lift coefficient, maximum lift angle of attack, etc.) can be used to construct continuous aerodynamic functions at any time. The primitives are adjusted by the model when the geometry varies or when flow conditions change, using a combination of physics-based scaling laws and empiricism. Section aerodynamics, for example, react to changes in size and flight condition, as they are corrected for compressibility via the Prandtl-Glauert transformation and for Reynolds number effects. Section aerodynamics are modified further as trailing edge flaps deploy.

Clean wing aerodynamics are computed from section performance based on its planform geometry, twist angle, and incidence angle. Stall angle, lift-curve slope, maximum lift coefficient, span efficiency, and other parameters are computed for the three-dimensional wing. Similar calculations are made for the flapped wing. Finally, overall three-dimensional vehicle aerodynamics are computed given fuselage, tail, and propeller information using an empirical drag buildup method.

4.2 Validation

The method is validated against the aerodynamics of a Fokker F27 turboprop transport reported in Reference 58. Like ORBET, the F27 is an unswept, high-wing transport driven by twin propellers. Though it is much larger, lacks a wing brace, and has a wing aspect ratio of only 12, the F27 otherwise bears an architectural similarity to ORBET. The aerodynamic model reacts to changes in size and geometry via physics-based and empirical relationships. Thus, if the model predicts the aerodynamics of the F27 closely, it is assumed that the aerodynamics of ORBET could be predicted by the same model with some confidence.

The F27 uses NACA series 64-421 sections at the wing root and thinner 64-415 sections at the tip (Ref. 59) and is equipped with single-slotted trailing edge flaps (Ref. 60). Flaps are estimated to occupy the rear 25 percent of the chord and are assumed to be extensible beyond the clean trailing edge by five percent (accuracy of these dimensions, of course, could be improved with access to more detailed data). Primitive characteristics for two-dimensional section aerodynamics at zero Mach number are obtained from the tool described in Reference 61. Three-dimensional vehicle-level aerodynamics are developed using the F27's gross geometry reported in Reference 59.

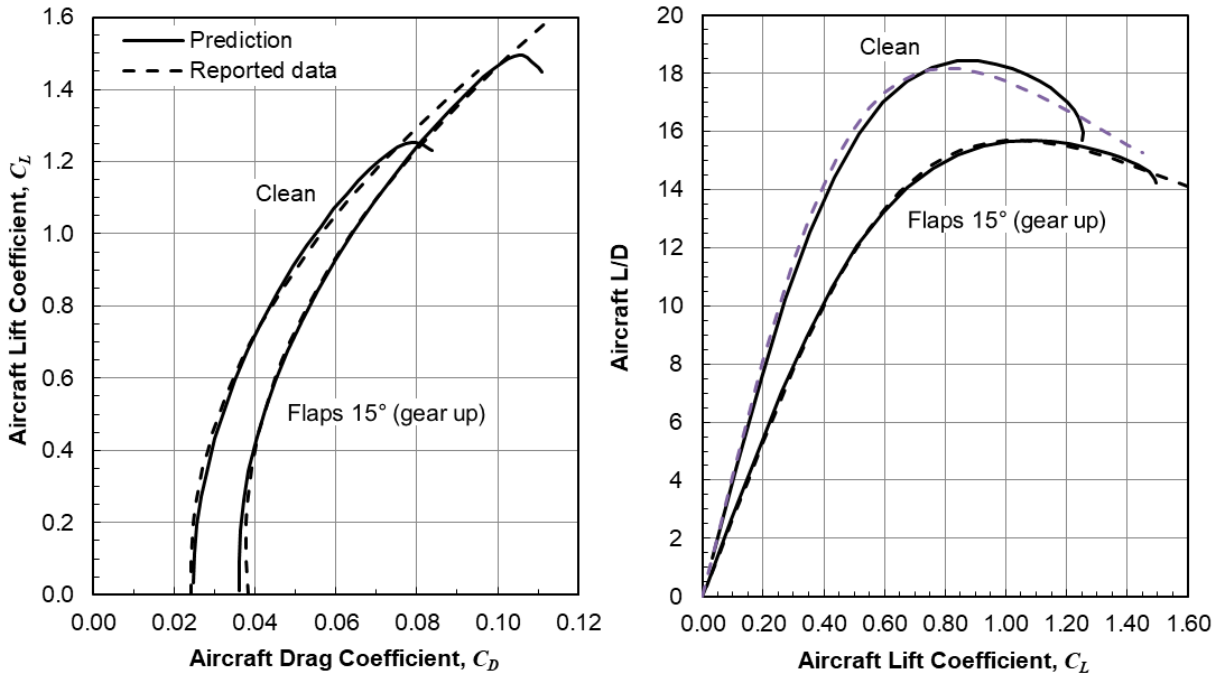

Figure 5.—Model validation of Fokker F27 aerodynamics.

The drag buildup procedure comes close to – but does not quite reproduce – the F27 reported data. To match the reported data, the zero-lift drag coefficient predicted by the model is adjusted slightly using a scalar calibration multiplier to match the data reported in Reference 58. Final calibrated aerodynamics are shown in Figure 5. Reported data are given by the dashed lines; the calibrated model prediction is given by the solid lines.

4.3 Use in ORBET Analysis

The same zero-lift drag calibration factor determined for the F27 is applied to ORBET. But there are other aerodynamic effects impacting ORBET. There is a drag penalty due to the wing brace as well as any of its associated interference drags. And with low airspeed (the unit Reynolds number per chord foot is just 1.5×10^6 ft^{-1}) and narrow wing chords, it might be reasonable to assume there is at least some natural laminar flow (Ref. 62). Very crudely, the benefit and penalty of these two competing effects are assumed to cancel each other exactly. Future work is needed to justify this assumption.

5.0 Propeller Model

5.1 Analysis Method

A propeller design and performance prediction model is required for the sizing and optimization process described in Section 7.0. The open-source software XROTOR (Ref. 63) is selected for the design and analysis of propellers. XROTOR requires just a fraction of a second to converge for any given design or performance calculation on a modern personal computer, making it well-suited for use in airplane sizing and optimization. As written, XROTOR is a menu-based code that relies on interactive user inputs.

A custom driver is written to communicate with XROTOR in batch mode. The driver is called repeatedly during sizing and optimization to design propellers and to compute their performance data.

The XROTOR design process begins with user-defined section aerodynamics for a set of two-dimensional airfoils. The sections are arranged into a spanwise propeller stack. Using an accounting similar to the airplane aerodynamic bookkeeping described in the preceding section, lift and drag coefficients of the sections are represented in the model by simplified characterization parameters, or primitives, rather than by continuously real functions. Section drag is scaled for Reynolds number effects as incoming flow conditions or chord lengths change. The airfoil sections are used to design a three-dimensional propeller. As typically used, the code computes the spanwise chord distribution at the aerodynamic design point. Chords are calculated at each station such that user-input design lift coefficient values are satisfied. Usually, the design lift coefficients are collectively expressed as a single major propeller design variable called the integrated design lift coefficient ($C_{Li,des}$), defined as $4\int_0^1 C_{li}(r)x^3dx$, where C_{li} is the local (section) lift coefficient at the design condition as a function of spanwise position r, and x is a dummy integration variable ranging from zero at the hub ($r = 0$) to unity at the tip ($r = R$), i.e., $x = r / R$. Note that other definitions of $C_{Li,des}$ exist in the literature. $C_{Li,des}$ is an indicator of overall blade camber and lift effectiveness.

Once determined, the chord distribution results in an activity factor per blade (*AF*), defined as $6250\int_0^1 (c(r)/D)x^3dx$, where c is the section chord as a function of spanwise position, r, and D is the propeller diameter. *AF* is a measure of the propeller's solidity. It is also considered to be a major propeller design variable. As of version 7.55, XROTOR does not compute *AF* from the chord distribution, but since the software is open-source, it is easily modified to do so.

Finally, most users opt to have the code compute the spanwise twist distribution. At the design point, twist angles are set to achieve a minimum induced loss circulation distribution (Ref. 64). Once the propeller is defined and performance is computed at its design condition, performance at any other off-design condition can be calculated.

5.2 Validation

Before XROTOR is used in this study, it is validated against experimentally measured propeller performance reported by United Technologies Corporation (Ref. 65). The experimental propeller has four blades, a 39 in. diameter, and a reported *AF* per blade of 91.

The family of HS-1 propeller airfoils (Ref. 66) is used for the propeller airfoil stack. Their spanwise locations are given in Reference 65. The airfoil family is shown in Figure 6 (for display purposes they are shown having identical chord lengths). No other geometry information is given in the reference.

The data in Reference 65 were obtained in United Technologies' Subsonic Wind Tunnel in East Hartford, Connecticut. Data were collected for ranges of airspeed, shaft power, shaft speed, and blade pitch angle. Results of the experiment are shown by the dashed lines in Figure 7. J is the dimensionless propeller advance ratio V / nD, where V is true airspeed, D is diameter, and n is shaft speed in revolutions per second. C_P is the dimensionless power coefficient $P / \rho D^5 n^3$, where P is the shaft power and ρ is ambient density. Efficiency is the dimensionless product of thrust and airspeed divided by shaft power. Efficiency contours from 85 to 90 percent are shown in the plot using increments of one percent. For the experimental data shown in the figure, airspeed was held at Mach 0.4 while shaft speed, shaft power, and blade pitch angle varied.

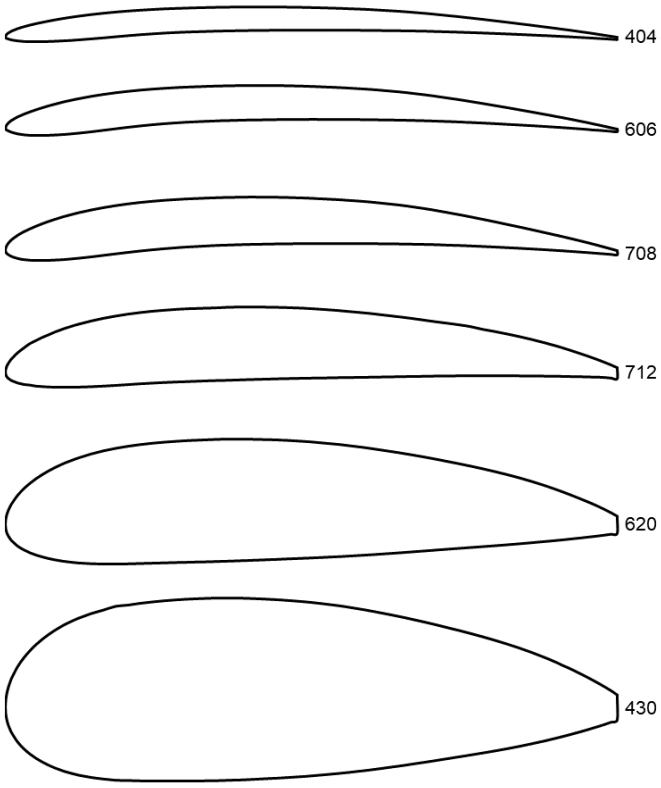

Figure 6.—United Technologies HS-1 propeller airfoil series.

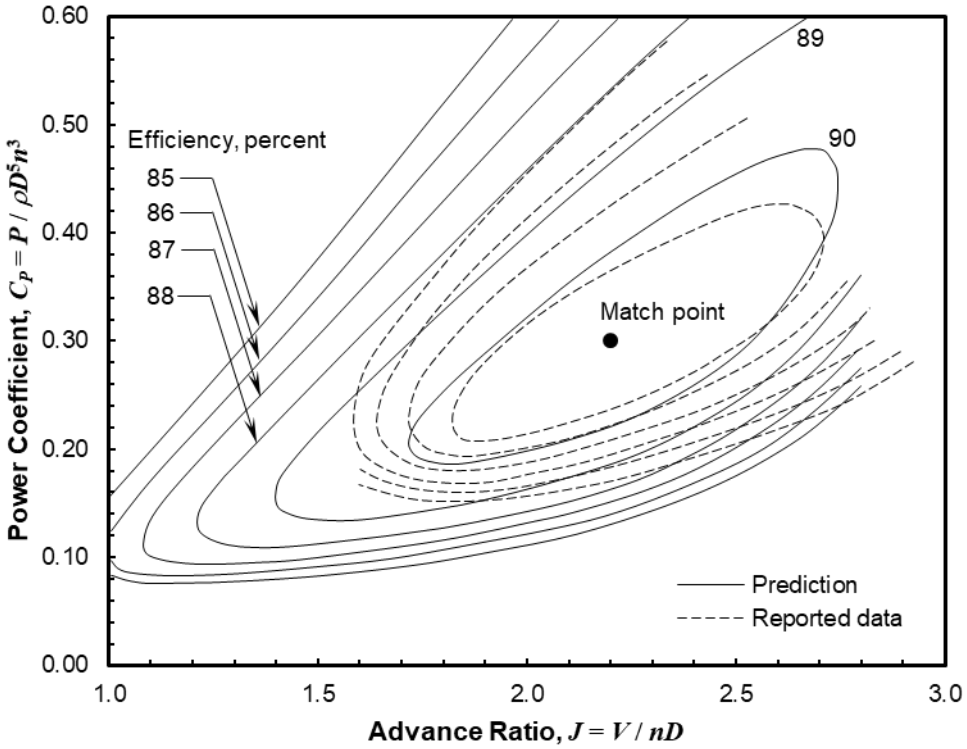

Figure 7.—Propeller performance map validation.

For the code validation, airfoil section aerodynamics are obtained from the tool described in Reference 61. An aerodynamic match point is selected using $J = 2.2$ and $C_P = 0.30$. Lacking additional geometric information for the propeller, two assumptions are required to set the chord and twist distributions. First, the propeller is designed iteratively by varying $C_{Li,des}$ until the activity factor converges upon 91, and second, the twist distribution is set via XROTOR's minimum induced loss optimization. XROTOR has a native feature for creating propeller performance maps, which has a design of experiments philosophy that differs from the wind tunnel measurements. In XROTOR, the ratio of wheel tip Mach number and J at the design point is held constant (i.e., the ratio of shaft speed squared and airspeed is constant everywhere on the map), while shaft power and blade pitch angle vary. In Figure 7, XROTOR's efficiency predictions are shown in solid lines. The efficiencies are not installed since no information about the experimental apparatus is known.

Differences in predicted vs. measured efficiency range from one to four percent across most of the performance map. Differences in efficiency are attributed to 1) approximate section aerodynamics, 2) unknown chord and twist distributions, 3) unknown installation effects, and 4) differences in the design of experiments.

5.3 Use in ORBET Analysis

In this study, XROTOR is used to design a propeller given a set of design variable values and to predict its off-design point performance. The family of HS-1 propeller airfoils (Ref. 66) is used for the propeller airfoil stack, and the spanwise chord and twist distributions are computed as discussed in the previous section. Uninstalled thrust and overall blade pitch angle are calculated given the independent variables of shaft power, shaft speed, and flight condition. Ordinarily, when a variable-pitch propeller is connected to a fuel-burning piston or a turboshaft engine, designers will fix shaft speed at a predetermined rate and use a constant-speed hub mechanism to maintain it. But in the case of an electric motor, shaft speed and shaft power can be readily uncoupled. A given amount of shaft power can be maintained over a selectable range of shaft speeds (the idea of an "electronic gearbox" is discussed more thoroughly in Section 9.0, where it is proposed as a low-noise operating mode for electric airplanes). For mission performance calculations, the maximum thrust occurring between 1100 rev/min and 1600 rev/min is used. Note that this technique could not be as easily replicated by a conventional system (at least, not without a variable-ratio gearbox), or by a constant-speed propeller. For any given propeller design, a table of thrust values as a function of flight condition and shaft power is assembled. The table is used as input to the mission performance calculations.

Propeller performance predictions need to be adjusted to account for blockage effects of downstream structures when installed on a vehicle. An installation method for tractor propellers adapted from FLOPS (Refs. 34 and 52) is used. The original reference is unknown, but the model format and thrust penalties are similar to the method reported in Chapter 6 of Torenbeek (Ref. 50) and elsewhere.

XROTOR is also able to design and analyze contra-rotation propellers by making flowfield adjustments. In a contra-rotation configuration, the aft propeller receives additional axial and rotational velocity components from the front propeller, while the front propeller receives an additional axial velocity component from the aft propeller. Each propeller is modeled in its own XROTOR simulation and flowfield information is passed from one simulation to the other. Iterations are required to converge on the final designs of each propeller. This capability is used to assess the ORBET variant shown on the right side of Figure 3. Implementation of this analysis is discussed in Section 8.0.

6.0 Vehicle Performance Model

6.1 Mission Calculations

With weight, aerodynamic, propeller, and energy models defined, airplane mission performance can be computed. The FLOPS performance tool (Ref. 34) is used. For ORBET, however, this cannot be done quite so straightforwardly as it is done for conventional fuel-burning airplanes.

Ordinarily, FLOPS operates under the assumption of variable airplane gross weight. As a conventional airplane burns fuel, it becomes lighter as the mission progresses. FLOPS capitalizes on this behavior to close the problem mathematically.

To accomplish this, FLOPS users are obliged to define a so-called “free cruise segment” somewhere in the principal mission. The amount of fuel and the distance flown in the free segment are initially unknown. The code computes performance from both ends of the mission, meeting at the beginning point and at the end point of the free segment. Starting with the ramp weight, performance is computed forward from taxi and takeoff until the beginning of the free segment is reached. Then, from the zero fuel weight, performance is computed from the reserve mission in reverse until the end of the free segment is reached. With the difference in fuel weight for the free segment known, its distance can be computed. A fuel-consistent mission is the result.

But an alternate approach is required to evaluate constant-weight airplanes like ORBET. With a few unconventional tactics, FLOPS can be persuaded into assessing fixed-weight airplanes. The basis for this is to assign a very small (but nonzero) amount of variable weight to the airplane. This weight is neither payload nor is it operating empty weight. Rather, it is akin to fuel weight in a traditional fuel-burning airplane. In the case of a constant-weight airplane, it must be small enough that it does not impact the performance of the airplane as it “burns off” during the mission, but it must be large enough to allow FLOPS to close the performance problem mathematically as described above. This “faux fuel weight” is on the order of 1 or 2 lb for ORBET.

To make use of the faux fuel weight, there must also be faux fuel flow rates. These fictitious rates are assigned to the powerplant performance data. Propeller thrust is a function of airspeed, altitude, and the shaft power consumption of the powerplants. Powerplant performance data consisting of installed thrust levels as a function of airspeed, altitude, and power consumption are contained in a file which is read by FLOPS in the usual manner. However, associated with every propeller thrust value must be a very small (but nonzero) faux fuel flow rate. This flow consumes the small amount of fuel weight that is assigned to the airplane. The mission is complete when the small weight of faux fuel is consumed and the free segment closes. The mission range becomes known and the overall weight of the airplane changes only inconsequently by 1 or 2 lb.

Although this enables constant-weight airplanes to be assessed, it is an arbitrary solution unless more information is applied. To accurately assess mission range, the energy used throughout the mission must match the total energy available from the batteries. Fortunately, FLOPS has two features that permit this to happen.

The first is the code’s ability to track an arbitrary propulsion variable as it changes throughout a mission. This feature was developed originally to track jet engine exhaust emissions throughout a mission, but it can be used to track any propulsion-related variable. Data for this variable are contained in the engine performance data file as a function of flight condition and power setting. If the propulsion variable is propeller shaft power, then a running total of energy consumed can be tracked throughout the mission. The total energy consumed is the sum of the energy consumed in each mission segment. The

second feature required is the code's ability to apply a scale factor to engine fuel flows. This feature was developed originally to explore sensitivities of vehicle performance with respect to engine efficiency. But for the case of constant-weight airplanes, the fuel flow scale factor can be adjusted iteratively until the energy used matches the energy available. A simple driver is developed for FLOPS to evaluate mission performance for ORBET in this manner.

6.2 Special Considerations for Part 23 Requirements

As already noted, FLOPS is principally a Part 25 tool intended for analysis of large, transport-category airplanes. As a smaller, Part 23 normal-category airplane, ORBET is required to comply with some airworthiness requirements that FLOPS is incapable of assessing unless it is modified.

Part 23 Level 4 multiengine airplanes like ORBET require a critical field distance calculation with one engine inoperative (also known as a balanced field length calculation), and must also meet subsequent climb gradient requirements. While FLOPS is indeed capable of computing critical field takeoffs, the takeoff speed requirements of Part 25 are more difficult to satisfy than those of Part 23. Part 25 requirements have additional minimum unstick-driven speeds that are not required by Part 23 (see 14 CFR§25.107 of Reference 47). Thus, using FLOPS to evaluate takeoffs without modification would be a very conservative option. It would result in field distances several hundred feet longer than the "actual" distance. Since (as will be shown later) the takeoff field distance is an active, binding constraint during sizing and optimization, this would adversely impact the solution. Takeoff distance calculations in FLOPS must be modified to accommodate ORBET.

In addition, minimum climb rate requirements after takeoff differ between Part 23 and Part 25, requiring more FLOPS modifications. For Part 23 airplanes, the climb requirements with all engines operating (given in section 23.2120(a) of Reference 14) as well as requirements with one engine inoperative (given in section 23.2120(b)(3)) are custom-programmed into FLOPS for this task. For all calculations with one engine inoperative, the engine-out yaw drag increment proposed by Torenbeek (Ref. 50) is used. Takeoff performance for ORBET is evaluated per section 23.2115(c) of Reference 14 for Level 4 airplanes using a sea level field with a 35 ft runway obstacle at standard (59 °F) conditions.

6.3 Energy Availability and Electrical System Technologies

Much like fuel in a conventional fuel-burning airplane, stored energy determines the range performance of an electric airplane. Stored energy in this study is modeled by a simple bookkeeping that is a function of 1) battery pack mass, 2) battery cell specific energy (i.e., the gravimetric energy density at the cell level, measured in W-h/kg), and 3) an energy conversion knockdown factor. The product of these three items determines the shaft energy available to the propellers.

The definition of the knockdown factor as used here requires discussion. Battery pack performance models often use cell performance as a starting point. In going from individual cells to the pack, losses in specific energy come from weight gains and energy losses. Specific energy at the cell level must be reduced to account for the weight of additional items within the battery pack beyond the battery cells. Most of the additional weight in the battery pack comes from the thermal management system, coolant, module housing structures, and additional electrical connectors. Cell specific energy is further degraded by electrical losses within the pack. The total reduction in specific energy – from the battery cells to the battery pack – is assumed to be 35 percent. Additional studies are required to justify this rough assumption.

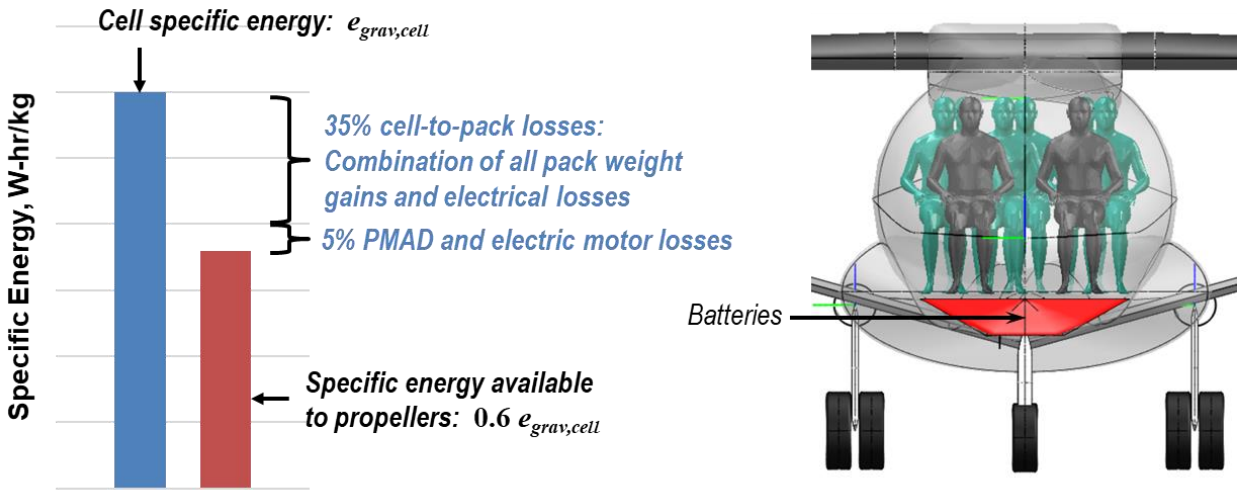

Figure 8.—Energy availability assumptions.

Between the battery pack and the propeller shafts there are additional energy conversion losses from the power management and distribution system and the electric motors. The total of these losses is assumed to be 5 percent. The weight of these items (i.e., W_{PMAD} and W_{motor}) is accounted for by the relations given in Section 3.0. Thrust is computed from shaft power and propeller efficiency as discussed in Section 5.0. This simple accounting is illustrated in Figure 8. Thus, the energy available to the propeller shafts is

$$E_{prop} = 0.6\, e_{grav,cell}\, W_{batt}$$

where $e_{grav,cell}$ is the gravimetric energy density at the cell level (converted to W-h/lb) and W_{batt} is the combined weight in pounds of the battery packs (determined as discussed in Section 3.0). Though it is a crude estimate, an overall electrical system knockdown factor of 0.6 is thought to be reasonable and perhaps conservative (e.g., Refs. 67 to 69).

Battery $e_{grav,cell}$ is treated as a technology parameter that is investigated for its influence on mission range. Once an optimum design is determined by the sizing process (discussed in the following section), $e_{grav,cell}$ is varied manually until the 250 nmi range goal is met. The value of $e_{grav,cell}$ required to meet the range goal is discussed in Section 8.0. The magnitude of $e_{grav,cell}$ indicates the technology required for ORBET's battery.

This energy accounting is very crude. Further, electrical component behavior, battery current discharge capability, and specific power are not considered. Ideally, batteries, electric motors, and the components making up the power management and distribution system should be modeled with more rigor. But this simple model allows quick calculations to be made, with the hope of a reasonable airplane design resulting in a short time. Future studies are needed so that energy and power requirements can be more accurately known. Additionally, it is possible for thermal loads to constrain airplane performance (Ref. 70), so the behavior of each electrical component should be built into the sizing process.

7.0 Sizing and Optimization

With propeller, weight, aerodynamic, and airplane performance discipline models defined, the airplane can be sized for optimum performance. Major design variables are identified and permuted by an optimizer so that mission range is maximized for a given value of $e_{grav,cell}$. Sizing and optimization is

limited to the single-rotation propeller variant. The contra-rotation propeller variant is assessed afterwards using the same airframe design as the single-rotation propeller variant.

7.1 Drivers and Optimizer

Drivers are constructed to execute each multidisciplinary model. A framework is used to pass information between analyses. The OpenMDAO framework and optimization software (Refs. 71 and 72) is used to model the process. OpenMDAO is an open-source computing environment and framework tool developed by NASA for multidisciplinary systems analysis and optimization. Components, groups and drivers are classes available in OpenMDAO to create objects. The objects are connected to form a sensible, multidisciplinary analysis of a problem. The models for propulsion, weight, aerodynamics, and vehicle performance represent independent subproblems having interrelated design and response variables. Each disciplinary model reacts to changes in design variables in the manner discussed above.

OpenMDAO supports a variety of optimization methods. Included are classical methods such as gradient-based methods, one direct (search-strategy) method, and evolutionary and particle swarm methods. With the number of optimization variables involved in this problem, it was hypothesized that the objective function might be discontinuous or beset by local optima, providing opportunities for gradient-based optimizers to become stuck. For this reason, a gradient-free particle swarm optimizer is used during initial sizing (the Augmented Lagrange Particle Swarm Optimizer, ALPSO (Ref. 73)). The design space is searched by ALPSO for feasible candidate designs. Simple penalty functions are used to constrain the optimum. ALPSO is used because it is expected to provide good results, largely without regard for its computational efficiency. The most attractive candidate design found by ALPSO serves as a starting point for the Sequential Least Squares Quadratic Programming optimizer (Ref. 74), which converges more precisely on the optimum.

7.2 Full Optimization Problem

The sizing and optimization problem is broken into two parts. A more complete, "full" statement of the problem is given first. The full problem is followed by an abridged problem, which is thought to be more tractable and practical for optimization. Design variables considered for the full optimization problem are listed in Table 1.

Most of the design variable definitions in the table are self-evident, but some require explanation. At the propeller design point, shaft power, P_{des}, and shaft speed, N_{des}, are specified at the flight conditions V_{des} and H_{des}. Note that the mission design variables $V_{cr,des}$ and $H_{cr,des}$ need not be equal to V_{des} and H_{des}.

Propellers powered by gas turbine engines or by reciprocating engines can be subject to a shaft power lapse with altitude. Propellers driven by electric motors and batteries have no such lapse unless, of course, power is deliberately reduced by the operator or by a control system. A feature of electric motors is that shaft speed can often be varied independently of shaft power. At least two additional design variables are needed to account for this added flexibility. For ORBET, the design variables P_{max} / P_{des} and N_{max} / N_{des} are introduced. These variables allow the propeller to operate with more power and/or rotational speed during takeoff and climb. For an all-electric airplane, adding shaft power during takeoff and climb mimics the natural thrust lapse of a naturally aspirated reciprocating engine or a gas turbine engine, but with more flexibility. The cruise phase requires much less power than the takeoff and climb phases. If ORBET's electric motors are to operate efficiently during each phase of flight, it may be advantageous to have "climb-assist motors" dedicated to takeoff and climb phases only. Each propeller could be driven by two electric motors. All of the motors would be used during takeoff and climb to maximize thrust. At the beginning of the cruise phase, the climb-assist motors would disengage. With such an arrangement, motor

efficiency during cruise could be higher than one large motor per propeller operating at reduced power. Dual electric motors are used on some series hybrid automobiles (e.g., Ref. 75).

Note that even the "full" design problem is simplified. Design variables pertaining to the fuselage, tail, high-lift flaps, and other systems are not identified in Table 1 since they are determined previously and separately by other requirements. And often, propeller details (e.g., airfoil stack, chord and twist distributions) and wing details (e.g., airfoils, chords, taper, sweep, twist, incidence) are considered in airplane design optimization. But for ORBET, they are demoted from design variable status by fiat. This is not to say that they are unimportant. Rather, in a conceptual design study, some variables may be excluded so that sizing can be simplified. A reasonable overall design can oftentimes be obtained by making reasonable simplifying assumptions.

Response variables computed from the design variables are listed in Table 2. J_{des} is the design propeller advance ratio, V / nD, where true airspeed, V, is expressed in feet per second, diameter, D, in feet, and shaft speed, n, in revolutions per second at the propeller design condition. (Note that in the literature, at least one other definition of J exists, where n is expressed in radians per second). $M_{hel,des}$ is the helical, or relative, propeller design tip Mach number. It is the root sum square of the tangential

TABLE 1.—DESIGN VARIABLES FOR FULL OPTIMIZATION PROBLEM

Propeller design variables	
D	Diameter, in.
B	Number of blades per propeller
P_{des}	Design shaft power, bhp (per powerplant)
N_{des}	Design shaft speed, rev/min
V_{des}	Design airspeed, kcas
H_{des}	Design altitude, ft
P_{max} / P_{des}	Ratio of maximum shaft power to design shaft power, > 1
N_{max} / N_{des}	Ratio of maximum shaft speed to design shaft speed, > 1
Wing design variables	
S	Reference area, ft^2
AR	Aspect ratio
δ_{flap}	Takeoff flap deflection angle, deg
Mission design variables	
$V_{cr,des}$	Design cruise airspeed, kcas
$H_{cr,des}$	Design cruise altitude, ft

TABLE 2.—RESPONSE VARIABLES

Propeller	
J_{des}	Design advance ratio
$M_{hel,des}$	Design helical tip Mach number
AF	Activity factor per blade
$C_{Li,des}$	Integrated design lift coefficient
P_{max}	Maximum shaft power, bhp (per powerplant)
N_{max}	Maximum shaft speed, rev/min
Vehicle	
R	Range, nmi
E_{tot}	Total mission energy available to propellers, kW-h
d_{to}	Critical takeoff field distance, ft
d_{land}	Landing field distance, ft
γ_{400}	Climb gradient at 400 ft altitude with one powerplant inoperative, percent
ROC_{svc}	Potential rate of climb at service ceiling, ft/min

(wheel) tip Mach number and the forward flight Mach number at the propeller design condition. *AF* is the activity factor per blade, and $C_{Li,des}$ is the integrated design lift coefficient as described in Section 5.0. *R* is the vehicle mission range with reserves as discussed in Section 6.0. E_{tot} is the total energy available to the propellers for the mission. d_{to} and d_{land} are the critical field distance and the landing field distance, respectively. γ_{400} is the climb gradient at 400 ft altitude with one powerplant inoperative. A discussion of how these values are computed for ORBET is found in Section 6.0. ROC_{svc} is the potential rate of climb at the service ceiling (i.e., at $H_{cr,des}$ and $V_{cr,des}$).

7.3 Design, Performance, and Behavioral Constraints

Optimization is subject to the following design, performance, and behavioral constraints:

1. $d_{to} \leq 4000$ ft and $d_{land} \leq 4000$ ft
2. $H_{cr,des} \leq 10{,}000$ ft and $H_{des} \leq 10{,}000$ ft
3. $ROC_{svc} \geq 300$ ft/min
4. $\gamma_{400} \geq 2$ percent
5. $V_{cr,des} \leq 250$ kcas and $V_{des} \leq 250$ kcas
6. $M_{hel,des} \leq 0.70$
7. $1.6 \leq J_{des} \leq 2.5$
8. $0.3 \leq C_{Li,des} \leq 0.8$
9. $80 \leq AF \leq 200$
10. $P_{max} / P_{des} \geq 1$
11. $N_{max} / N_{des} \geq 1$
12. $AR \leq 19$

The first five constraints are performance requirements defined for the vehicle. The limits assigned to d_{to}, d_{land}, $H_{cr,des}$, and H_{des} were discussed in Section 2.0. d_{to} and d_{land} are computed for a sea level field at 59 °F, standard day conditions. ROC_{svc} is evaluated at $H_{cr,des}$ and $V_{cr,des}$. For Level 4 category multiengine airplanes like ORBET, the minimum γ_{400} allowed is 2 percent, and limits for $V_{cr,des}$ and V_{des} are set to 250 kcas, the upper limit of low-speed category airplanes (see 14 CFR§23.2005 and 14 CFR§23. 2120(b)(3) of Reference 14. The next six constraints are limits for typical low-speed propellers. A modest upper limit is chosen for $M_{hel,des}$ in anticipation of noise requirements (though noise is not explicitly evaluated in this study). It is also chosen in anticipation of propeller airfoil selection (discussed in the following section). The final constraint is the upper limit for *AR*. It is set to 19: the aspect ratio reported for the Transonic Truss-Braced Wing concept developed by Boeing (Refs. 76 and 77). This constraint is somewhat arbitrary. Higher values of *AR* might be possible, provided the weight increase can be properly computed (the method in Reference 34 is valid for aspect ratio values up to 25), and if there are no aeroelastic or structural issues. This limit is viewed as a non-mandatory, flexible constraint for an unswept, low-speed, braced wing for an airplane like ORBET.

7.4 Abridged Optimization Problem

Simplifications are made to the full optimization problem given above to reduce the number of design variables. The intent is to make the problem more tractable and practical for optimization. The resulting eleven design variables are shown in Table 3.

TABLE 3.—DESIGN VARIABLES FOR THE OPTIMIZATION PROBLEM

Propeller design variables	
P_{des}	Design shaft power, bhp (per powerplant)
N_{des}	Design shaft speed, rev/min
V_{des}	Design airspeed, kcas
H_{des}	Design altitude, ft
$C_{Li,des}$	Design integrated lift coefficient
P_{max} / P_{des}	Ratio of maximum shaft power to design shaft power
N_{max} / N_{des}	Ratio of maximum shaft speed to design shaft speed
Wing design variables	
S	Wing reference area, ft^2
AR	Wing aspect ratio
δ_{flap}	Takeoff flap deflection angle, deg
Mission design variable	
$V_{cr,des}$	Design cruise airspeed, kcas

The abridged list is the result of the following simplifications:

1. The propeller diameter, D, is set by a disk loading assumption. Torenbeek (in Chapter 6 of Reference 50) provides a regression model for propeller disk loading (P_{max}/A_{prop}, or $4P_{max}/\pi D^2$) for a variety of airplanes powered by reciprocating and turboprop engines. The correlating variable is $(P_{max}V_{cr})^{0.5}$, for reasons explained in the reference. Torenbeek's regression curve and his data are reproduced in Figure 9, with the disk loading of the final, optimized single-rotation ORBET variant located on the curve.
2. The number of propeller blades, B, is set to five. The relatively high blade count is chosen for its generally positive influence on performance, noise and vibration.
3. The family of United Technologies Corporation HS-1 propeller airfoils (Ref. 66) described in Section 5.0 is used for the propeller airfoil stack. These airfoil sections have good lift performance during takeoff and climb, good lift-to-drag ratio in cruise, and they are popular in low-speed applications. The propeller helical tip Mach number, M_{hel}, is modest to avoid supersonic flow on the upper blade surfaces. Section aerodynamics are computed using the tool in Reference 61. Airfoil sections are assigned to the spanwise locations suggested in Reference 65.
4. The XROTOR tool (Ref. 63) is used to set the propeller spanwise chord distribution based on the input design integrated lift coefficient, $C_{Li,des}$. Put another way, $C_{Li,des}$ is a design variable that replaces the need to specify the propeller chord distribution.
5. The XROTOR tool is allowed to set the propeller spanwise twist distribution such that induced loss is minimized at the design condition (Ref. 64).
6. The NACA 64-421 airfoil section is used from the wing root to the propulsion pod. The thinner NACA 64-415 airfoil section is used from the pod to the tip. Section aerodynamics are computed using the tool in Reference 61.
7. The wing is a basic trapezoid with a taper ratio of 0.42, wing twist washout angle of 1.25°, and quarter chord sweep of 1.6°. These are reasonable values for a low-speed application.
8. $H_{cr,des}$ is set to 10,000 ft (the maximum allowed). This is based on observations made during preliminary optimizations which determined that airplane range is always maximized at that condition.

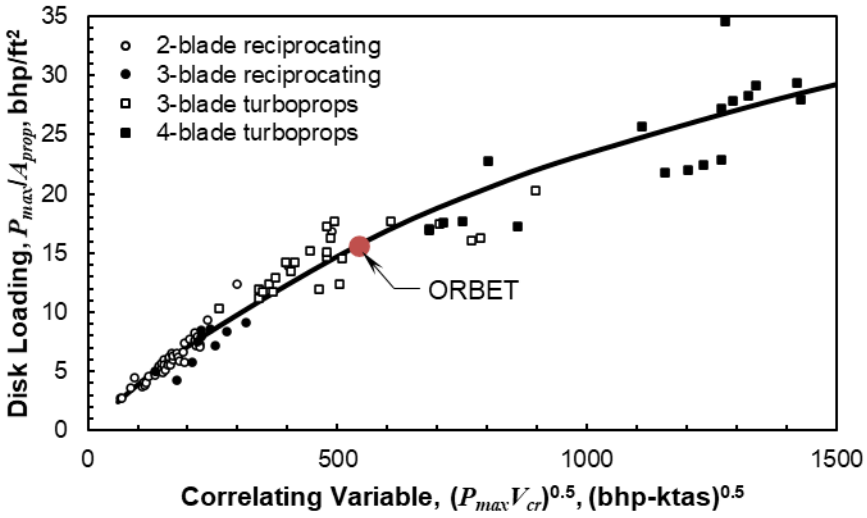

Figure 9.—Propeller disk loading model, adapted from Reference 50.

Using the propeller disk loading characteristic (adapted from Reference 50 and shown in Figure 9) does not mean that propeller diameter is neglected in the abridged optimization. Rather, it is equivalent to addressing diameter inside a nested optimization subloop under the top-level optimizer. But instead of subjecting diameter to a formal suboptimization, it is set directly by the empirical disk loading characteristic, where optimization has been done previously for other propeller designs. From actuator disk theory, it can be straightforwardly shown that efficiency is a function of disk loading, and that as design airspeed increases, higher disk loadings are generally required. So the independent variables in the correlating variable (i.e., maximum shaft power, P_{max}, and true cruise airspeed, V_{cr}, are sensibly chosen: it is reasonable to assume that the optimum disk loading is proportional to $P_{max}V_{cr}$. The correlation of data plotted in Figure 9 seems to justify the assumption. So stated another way, replacing diameter optimization with a disk loading characteristic is like relying empirically on a set of historical diameter optimizations – with respect to P_{max} and V_{cr} – made by others for different applications in the past.

Similarly, allowing XROTOR to set the spanwise chord and twist distribution is not neglecting them in the abridged optimization. Instead, they are addressed in a nested subloop where they are optimized for minimum induced loss and to meet lift requirements set by $C_{Li,des}$. The end result of these simplifications is to reduce the burden on the top-level optimizer, making the problem more tractable and practical.

7.5 Formal Statement of the Abridged Optimization Problem

The abridged ORBET sizing and optimization problem consists of ten design variables. An extended design structure matrix diagram (XDSM, (Ref. 78)) of the abridged problem is shown in Figure 10. The design variables may pertain to one of the four local disciplinary analyses, or they may be among those shared globally by multiple disciplines. Design variables are contained either in the vector of shared global variables, $\boldsymbol{x}_0$ (having a zero subscript), or in one of the local discipline vectors, $\boldsymbol{x}_1$ through $\boldsymbol{x}_4$, with the subscript denoting the disciplines of propellers, weights, aerodynamics, and performance, respectively. The vector $\boldsymbol{x}$ (without extra notation) contains all of the design variables (i.e., $\boldsymbol{x} = [\boldsymbol{x}_0{}^T, \boldsymbol{x}_1{}^T, \boldsymbol{x}_2{}^T, \boldsymbol{x}_3{}^T, \boldsymbol{x}_4{}^T]^T$). The vector of initial values of $\boldsymbol{x}$ is denoted by $\boldsymbol{x}^{(0)}$.

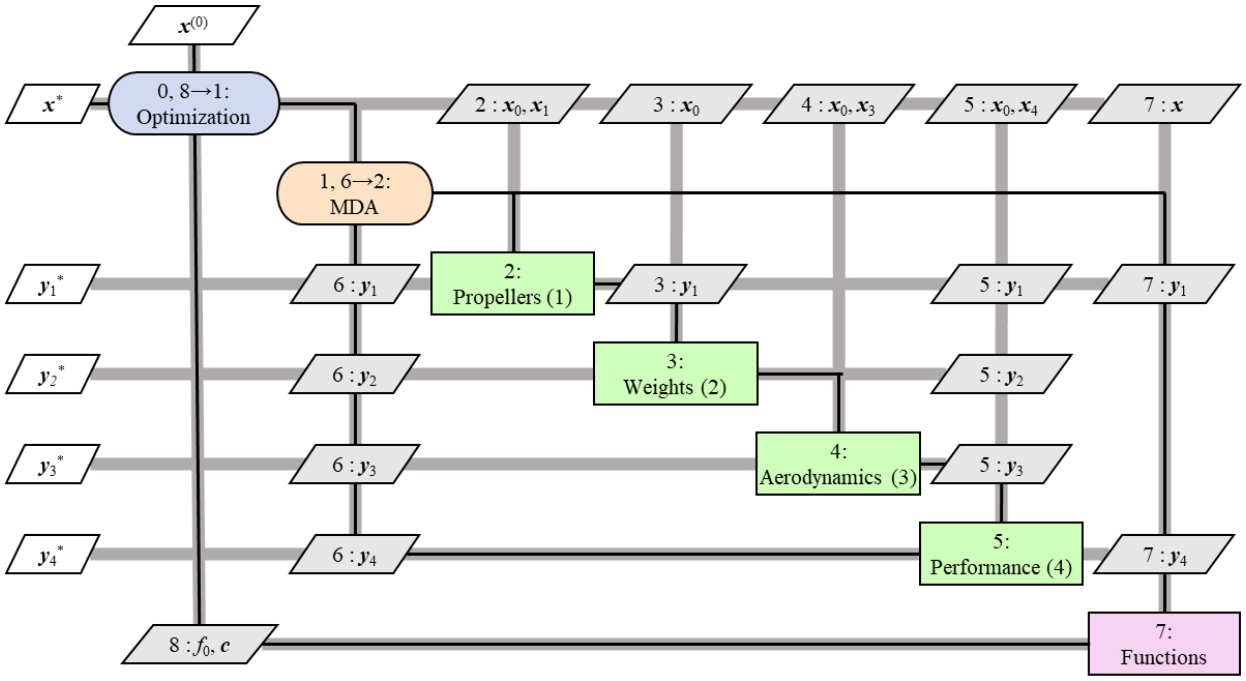

Figure 10.—Extended design structure matrix (XDSM) diagram of abridged optimization problem.

TABLE 4.—SIZING AND OPTIMIZATION VARIABLES

Design variables:

Vector	Discipline	Contents
$\boldsymbol{x}_0$	Shared	[S, AR, V_{des}, H_{des}]
$\boldsymbol{x}_1$	Propellers	[P_{des}, N_{des}, $C_{Li,des}$, P_{max}/P_{des}, N_{max}/N_{des}]
$\boldsymbol{x}_2$	Weights	[]
$\boldsymbol{x}_3$	Aerodynamics	[δ_{flap}]
$\boldsymbol{x}_4$	Performance	[$V_{cr,des}$]

Response variables:

Vector	Discipline	Contents
$\boldsymbol{y}_1$	Propellers	[D, P_{max}, N_{max}, AF, J_{des}, $M_{hel,des}$, performance data]
$\boldsymbol{y}_2$	Weights	[E_{tot}]
$\boldsymbol{y}_3$	Aerodynamics	[aerodynamic data]
$\boldsymbol{y}_4$	Performance	[R, d_{to}, d_{land}, γ_{400}, ROC_{svc}]

Using the same subscripts, response variables computed by each discipline analysis are contained in the vectors $\boldsymbol{y}_1$ through $\boldsymbol{y}_4$. A vector of design constraints (given in Section 7.0) is denoted by $\boldsymbol{c}$. The objective function, f_0, is the negative of mission range, R, to be minimized. The shared objective, f_0, is a function of design variables ($\boldsymbol{x}$) and response variables ($\boldsymbol{y}$, which are in turn functions of $\boldsymbol{x}$). Design variables or response variables at their optimal value (i.e., when f_0 is optimal) have asterisk superscripts. Design variables can be under manual control or they may be under control of the optimizer. These two analysis modes are indicated by the multidisciplinary analysis (MDA) path or the optimization path in the diagram, respectively. Design variables and response variables corresponding to those in the diagram are shown in Table 4.

Note that the local design variable $\boldsymbol{x}_2$ is a zero vector (i.e., a vector of length zero), since the weight discipline uses response variables and shared design variables as inputs. Also note that the responses from the propeller analysis ($\boldsymbol{y}_2$) and the aerodynamic analysis ($\boldsymbol{y}_3$) contain tabular data files. Propeller performance data consisting of thrust and shaft power are predicted as functions of altitude and airspeed. Aerodynamics consisting of lift and drag coefficients are predicted as functions of angle of attack, flap deflection angle, and Reynolds number. These sets of tabular data are required for the vehicle mission performance analysis. New sets of tabular data files are computed and used in the performance analysis whenever design variables change.

All design variables are optimized together at once rather than in parallel or nested groups. That is, the optimization occurs in series, with each disciplinary subproblem executed whenever one or more of its design variables are changed. The optimizer is relied upon to discover a feasible solution with sensible design values for each disciplinary subproblem. The propeller design subproblem, for example, is optimized with respect to mission range. Classical propeller design optimizations often used propeller-centric aerodynamic metrics such as efficiency as a sole objective. Such designs were often based on the theories of Betz (Ref. 64). But there are usually competing performance requirements such that propeller designs for best cruise efficiency and propeller designs for best takeoff and climb performance are different. Recommended propeller design practices for these types of problems are summarized in Reference 79, for example. More recently, there have been multidisciplinary propeller optimizations that account for the entire vehicle (e.g., Ref. 80). Optimization considering multiple disciplines is important because the goal is often more complex than simply maximizing propeller efficiency or thrust. ORBET's sizing is a mixed-variable multidisciplinary optimization problem, where airframe and propeller variables are optimized jointly.

A formal statement of the problem can be written as:

Minimize $f_0(\boldsymbol{x}, \boldsymbol{y}(\boldsymbol{x}))$
With respect to $\boldsymbol{x}$
Subject to $\boldsymbol{c}$

The constraints in $\boldsymbol{c}$ are formulated so that they contribute to the simple penalty function on f_0 used by the particle swarm optimizer. The compound inequalities for J_{des}, $C_{Li,des}$, and AF are each broken into two simple inequality constraints. Design variables are scaled so that their magnitudes are on the order of unity.

As discussed above in Section 6.0, battery cell specific energy, $e_{grav,cell}$, is treated as a system technology parameter. That is, it is not a continuous-real design variable that changes during a sizing analysis. Rather, it is treated as a constant in any given sizing and optimization, but it may be changed for other optimizations. It is varied manually after the optimization is complete until the 250 nmi range goal is met. Alternately, the optimization problem could be reformulated to minimize $e_{grav,cell}$ subject to a range constraint, but that would increase the cost of optimization.

8.0 Candidate Airplanes

8.1 Single-Rotation Propeller Variant

Optimized design variables for the single-rotation propeller variant (see Figure 3, left) are given in Table 5. Other characteristics of the design are shown in Table 6. Batteries are predicted to weigh 6622 lb. As discussed in Section 6.0, specific energy at the cell level ($e_{grav,cell}$) is a system parameter that indicates the level of battery technology needed to meet the goal mission range. For the design case, $e_{grav,cell}$ is varied so that the range (with 45 min reserves) is 250 nmi. For this range, the batteries are

TABLE 5.—OPTIMIZED DESIGN VARIABLES

P_{des}, bhp	587	N_{des}, rev/min	1170
V_{des}, ktas (kcas)	250 (216)	H_{des}, ft	10,000
$C_{Li,des}$	0.350	P_{max} / P_{des}	2.00
N_{max} / N_{des}	1.37	S, ft^2	317
AR	19.0	δ_{flap}, deg	16
$V_{cr,des}$, ktas (kcas)	180 (155)	————	---

TABLE 6.—CHARACTERISTICS OF THE DESIGN

Vehicle		**Power**	
Maximum gross weight, lb	18,000	Cruise motors, kW	210
Payload weight, lb	3800	Climb-assist motors, kW	670
Battery pack weight, lb	6622	Overall electrical system knockdown factor	0.6
Thrust loading (sea level, static)	0.508	Specific energy (cell, $e_{grav,cell}$), W-h/kg	600
Wing loading, lb/ft^2	56.8	Specific energy (system, 0.6 $e_{grav,cell}$), W-h/kg	360
Wingspan, ft	77.6	Total mission energy, kW-h	1081
Propellers		**Performance**	
D, in. (area, A_{prop}, ft^2)	118 (75.3)	Cruise altitude, ft	10,000
AF (per blade)	85.4	Cruise airspeed, ktas (kcas)	180 (155)
J_{des}	2.21	Cruise lift-to-drag ratio	20.5
$M_{hel,des}$	0.681	Critical field distance (sea level, 59 °F), ft	4000
N (sea level, static), rev/min	1600	Takeoff distance to 35 ft (sea level, 59 °F), ft	2750
Installed thrust (sea level, static), lb	4569	Range (with 45 min reserves), nmi	250

required to supply 1081 kW-h of energy. If the batteries are to occupy the 150 ft^3 volume underneath the cabin floor, they would require a volumetric energy density of 420 W-h/l at the pack level. Packaging batteries into this volume seems practical at today's technology levels (e.g., Ref. 69).

Cell specific energy, however, is a different matter. The requirement for $e_{grav,cell}$ to meet the range goal is 600 W-h/kg. This is more than twice the specific energy of modern Type 2170 Lithium-ion (Li-ion) cylindrical cells in use by Tesla (e.g., Ref. 69). Doubling the specific energy of Li-ion batteries is doubtful (Ref. 81), so substantial specific energy gains for batteries using this chemistry seem unlikely. An all-electric airplane of this type and with these performance requirements seems limited by today's Li-ion battery technology. But increases in battery cell specific energy may be possible with other battery chemistries. Laboratory experiments on Lithium-Sulfur (Li-S) batteries show promise of reaching in the near term the specific energy levels required by ORBET (e.g., Refs. 82 to 84). And battery manufacturers Sion Power and Oxis Energy expect that future Li-S cells will have specific energy levels of up to 600 W-h/kg (Ref. 85). Provided that issues such as poor cyclability, anode corrosion, and the low electrical conductivity of sulfur can be resolved, Li-S batteries could improve prospects for transports like ORBET.

Three variables are at their assigned limits. The design variables, AR and H_{des}, have values of 19 and 10,000 ft, respectively. The response variable, d_{to}, has a value of 4000 ft. Solutions having optimized design variables at their limit is a possible cause for concern. As discussed earlier, however, the limit for AR is viewed as non-mandatory or flexible. Further study is required to determine the influence of higher values of AR on wing weight and aerodynamics, and the influence of higher values of H_{des} on propeller performance.

The optimized propeller design airspeed, V_{des}, of 250 ktas (or 216 kcas when H_{des} is 10,000 ft) is seemingly odd considering that ORBET never exceeds 180 ktas in its design mission. But this is a consequence of relying on an optimizer to design a propeller that performs well at takeoff, climb, and during cruise. The propeller design point has a high efficiency, but it occurs at an advance ratio where the propeller ordinarily never operates (shown in the propeller performance map in Figure 11). Nonetheless, the propeller's design is such that it provides good overall performance during all phases of the design mission. Uninstalled propeller performance data are shown in Table 7. An alternate 250 ktas high-speed cruise condition is also shown in the figure and in the table, but it is not part of the design mission. Though the high-speed cruise condition enjoys a higher propeller efficiency, flying at 250 ktas requires considerably more power than flying at 180 ktas, and it results in a lower cruise lift-to-drag ratio and less range.

The active constraint for the critical field length, d_{to}, is perhaps the most impactful. Without a field distance requirement, ORBET's required thrust and wing area could be much lower before other constraints become active, resulting in better performance. This is a classic airplane sizing problem: if wings are sized for efficient cruising at a high lift-to-drag ratio, then takeoff and climb requirements often go unmet. In the case of ORBET, a solution for P_{max} / P_{des} and N_{max} / N_{des} is found that allows its propellers to operate with more power and rotational speed during takeoff and climb. This behavior mimics the natural thrust lapse of a reciprocating or a gas turbine engine. ORBET's powerplant has greater operational flexibility than a fuel-burning engine, since it is not limited to a natural thrust lapse.

Indeed, since shaft power and shaft speed are readily uncoupled for electric motors, propeller thrust can be optimized somewhat for any given shaft power and flight condition. In the case of ORBET, this is accomplished as discussed in Section 5.0. In a real airplane, this additional benefit would be implemented using a full-authority digital system that controls propeller pitch and shaft speed.

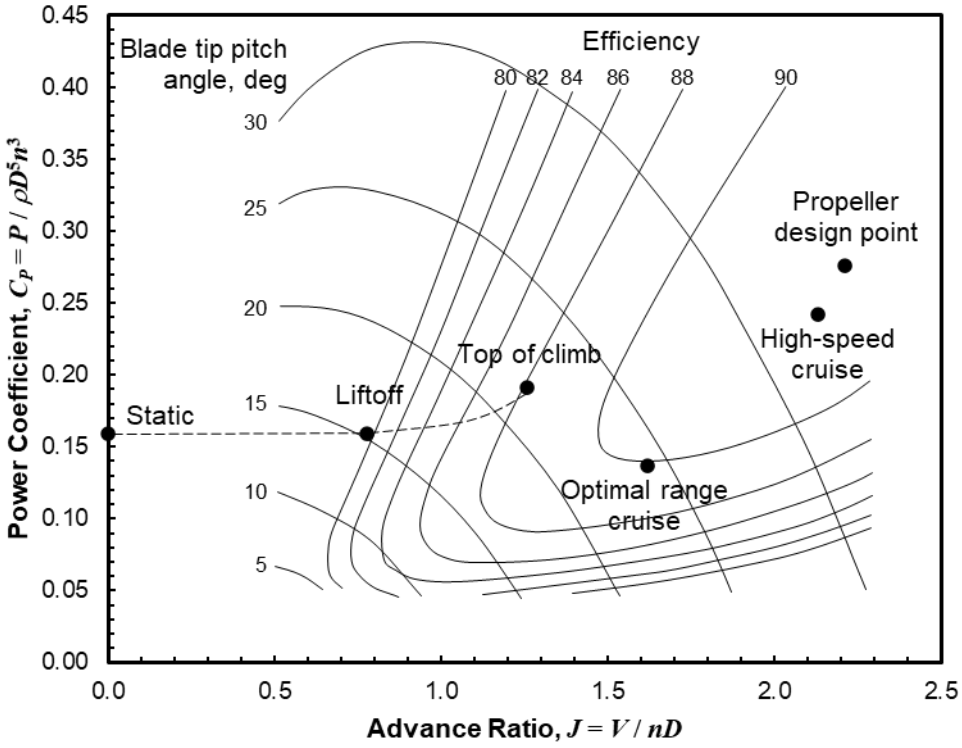

Figure 11.—Single-rotation propeller performance map.

TABLE 7.—UNINSTALLED PROPELLER PERFORMANCE AT SELECT CONDITIONS

	Design	Static	Liftoff	Top of climb	Optimal range cruise	High-speed cruise
P, bhp	587	1174	1174	822	277	576
P/A_{prop}, bhp/ft^2	7.80	15.6	15.6	10.9	3.7	7.6
N, rev/min	1170	1600	1600	1480	1150	1210
V, ktas (kcas)	250	0	120	180	180	250
H, ft	10,000	0	0	10,000	10,000	10,000
$J = V / nD$	2.21	0	0.776	1.258	1.619	2.13
M_{hel}	0.681	0.735	0.757	0.758	0.615	0.698
$C_P = P / \rho D^5 n^3$	0.276	0.159	0.159	0.191	0.137	0.242
$C_T = T / \rho D^4 n^2$	0.114	0.298	0.164	0.134	0.076	0.104
$\eta = JC_T / C_P$	0.913	0	0.796	0.882	0.899	0.912
Thrust, lb	699	4631	2540	1313	450	686

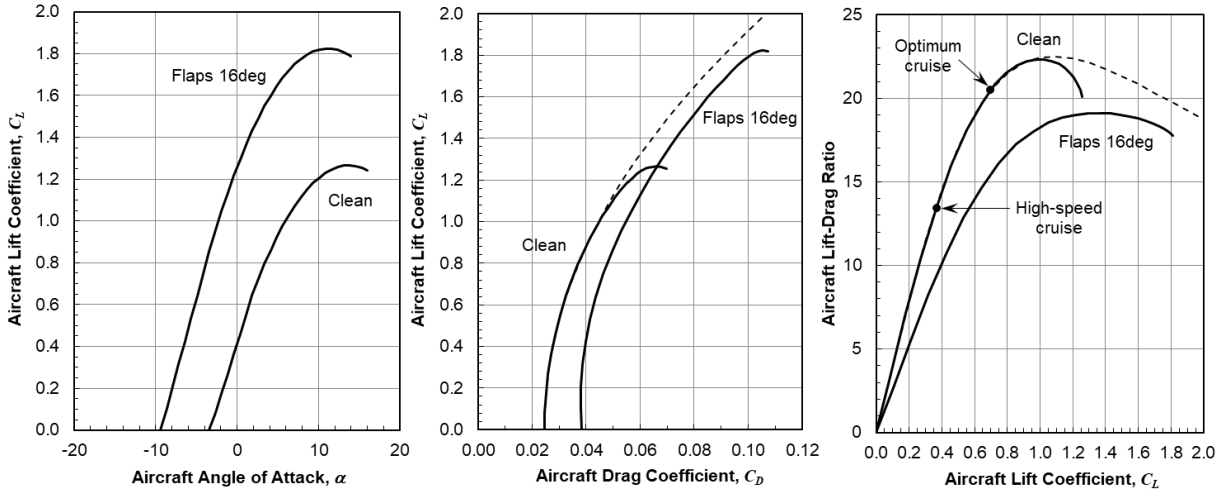

Figure 12.—Airplane aerodynamics.

For ORBET, the cruise motors and climb-assist motors (described in Section 7.0) could be rated at 210 and 670 kW, respectively. During descent, it is possible that the motors could act as generators to charge the batteries. This energy recuperation technique – sometimes called “energy harvesting” – is not studied here.

In addition to the 4000 ft critical field distance, the takeoff distance to a 35 ft obstacle with all engines operating is of interest. From a sea level field at 59 °F, this distance is 2750 ft. This allows ORBET to operate from most runways. Airplane aerodynamics for the optimized design in clean and takeoff configurations are shown in Figure 12. A weight statement is shown in Table 8. Sensitivity studies using this variant are discussed in Section 8.3.

TABLE 8.—WEIGHT STATEMENT (WEIGHTS IN POUNDS)

Wing	1479
Horizontal tail	140
Vertical tail	125
Fuselage	1827
Landing gear	639
Nacelles	199
Structure total	4409
Electric motors	385
Propellers	345
Battery packs	6622
Propulsion total	7352
Surface controls	163
Hydraulics	147
Power electronics	593
Avionics	235
Furnishings and equipment	840
Anti-icing	50
Systems and equipment total	2028
Weight, empty	13,789
Flight crew (2) and baggage	410
Operating weight, empty	14,199
Passengers (19)	3230
Passenger baggage	570
Maximum takeoff gross weight	18,000

8.2 Contra-Rotation Propeller Variant

A contra-rotation propeller (Figure 3, right) is assessed using the method described in Section 5.0. It is installed on the vehicle optimized for the single-rotation propeller. No additional vehicle optimization is performed. In a contra-rotation configuration, the rear propeller receives the flowfield created by the front propeller. The aft row turns rotational flow back into the streamwise direction. Isolated efficiency of the aft row decreases with increasing flowfield speed, but the overall efficiency (considering both rows) may increase due to recovery and conversion of swirl losses into useful forward thrust. Properly designed, swirling flow and torque reaction of a contra-rotation propeller will be near zero. Reducing swirling flow on the vertical tail also can improve handling qualities at lower speed. A contra-rotation configuration seems attractive for propellers driven by electric motors due to the comparative ease of implementation. Two electric motors could straightforwardly be arranged to drive forward and aft propellers, whereas contra-rotation propellers driven by reciprocating engines or by gas turbine engines require elaborate geartrains or contra-rotating power turbines.

Aircraft with contra-rotation propellers have been mass-produced principally by the United Kingdom and by Russia or the former Soviet Union. Examples are military transports such as the Tupolev Tu-95, Antonov An-70, Avro Shackleton, and Fairey Gannet. Few civil passenger transports have been equipped with contra-rotation propellers. Perhaps the most notable was the Tupolev Tu-114 passenger transport (developed from the Tu-95). A Ukrainian civil version of the An-70 is a convertible cargo/passenger

transport that can be equipped with seats in removable modules. Cancelled civil programs include the Bristol Type 167 Brabazon and the Douglas DC-8 piston-engine airliner.

Contra-rotation propellers have different noise characteristics than single-rotation propellers. Perhaps chief among the differences are additional discrete interaction tones and their harmonics created by trailing edge wakes departing the front propeller and being intercepted by the aft propeller. Thus, contra-rotation propellers can be particularly rich in tone content. In instances where the tones occur at similar frequencies, they can be strengthened via constructive reinforcement or be reduced via destructive cancellation (which was recognized perhaps as early as 1948 (Ref. 86)). Contra-rotation propellers can be noisier in the axial direction (e.g., Ref. 87). But they can be made quieter if noise mitigation strategies are used. Unequal blade counts or shaft rotational speeds can change the strength of discrete interaction tones (Refs. 88 and 89), which could be accomplished easily in an electric motor-driven application such as ORBET with independent shaft speed control. Other known noise mitigation strategies for contra-rotation propellers include aeroacoustic blade shaping, blade pitch angle and rotational speed optimization, increased blade counts, low disk loading, blade spacing optimization, and aft blade clipping (Ref. 90).

In this study, a contra-rotation propeller is designed very simply without a great deal of rigor using many characteristics taken from the optimized single-rotation propeller. Shaft power of a single propeller is divided equally between two propellers (each absorbing P_{max} / 2), rotating in opposite directions. For each propeller, values for C_P, J, and M_{hel} at the aerodynamic design point (V_{des} and H_{des}) are maintained, as are the number of blades and the design variables $C_{Li,des}$, P_{max} / P_{des}, and N_{max} / N_{des} (see Table 5 and Table 7). These propellers are designed using the XROTOR tool in the presence of interdependent flowfields calculated as described in Section 5.0. New twist and chord distributions are computed for front and aft propellers. To maintain comparable thrust performance, blade diameters of both blade rows are reduced equally until the uninstalled design thrust of the contra-rotation propeller is identical to the single propeller.

This simplistic design approach results in little performance improvement. Uninstalled efficiency at the aerodynamic design point increases by less than one point. Propeller weight increases by 25 percent for the contra-rotation configuration. When mission performance is evaluated, there is virtually no net range benefit. This may come as a surprise, given some of the efficiency increases reported for contra-rotation propellers (e.g., Ref. 91). Part of the explanation for the disappointing performance is certainly due to the simplistic design approach used here. In contra-rotation configurations, the blade rows are in flowfields that differ from the freestream. Compared to the isolated case, the forward propeller receives higher axial velocity, provided the blade rows are sufficiently close. More importantly, the downstream propeller receives higher axial velocity and an additional rotational flow component. Since the resultant velocities are higher for the aft propeller, and if given the same lift requirement as the front propeller, its chords should be generally narrower than the front propeller. And if optimized for minimum induced loss, the aft propeller should have less twist than the front propeller. But in this study, each propeller is designed for minimum induced loss separately, rather than as a system. Additional benefit might be realized if spanwise chord and twist distributions are set as a system, and if additional design variables are introduced.

But, the disappointing performance of the contra-rotation propeller might be explained more simply: there may not be enough swirl to justify its removal. Given ORBET's low speed, the optimal design for its single-rotation propeller has a rather low disk loading and a very high efficiency. Relative to more highly loaded propellers, a propeller with lower loading and higher efficiency imparts comparatively little rotation to its wake. The swirl losses introduced by the front propeller may not be great enough to justify a contra-rotating aft propeller. Dramatic efficiency gains attributed to contra-rotation in the literature are often for propellers with disk loadings three or four times higher than ORBET.

8.3 Sensitivity Studies and Alternative Designs Using the Single-Rotation Variant

Several sensitivity studies and alternative designs are performed using the single-rotation propeller variant as described in this section. In all cases, the design variable values shown in Table 5 are unchanged, though other aspects of the vehicle or the way it is used are changed.

8.3.1 Payload-Range Performance

A traditional payload versus range diagram is shown in Figure 13 (left). It is rather unlike similar diagrams for fuel-burning airplanes, where gross weights increase as fuel and/or payload is added to their operating empty weights. In the case of ORBET, battery weight remains constant despite its state of charge, so the only instance when gross weight changes is when payload weight changes. Thus, there are only two linear segments in ORBET's diagram. The horizontal segment occurs at maximum payload weight (3800 lb) and at maximum gross weight (18,000 lb) as the state of charge varies. The descending segment occurs as payload is offloaded. Gross weight falls to 14,200 lb for the case of a self-ferry mission, where range with reserves increases from 250 nmi at the design point to 301 nmi.

Other ORBET variants are possible if passengers and their baggage are replaced by additional batteries, as shown in Figure 13 (right). For these alternative configurations, maximum gross weight is held constant at 18,000 lb in all instances, but battery weight is allowed to increase from 6622 lb as payload is reduced. The additional batteries (provided that interior volume can be found for them) allow more mission energy to be stored so that range may be improved. Note that with maximum seating for less than ten passengers, ORBET would fall into a different classification type (see 14 CFR§23.2005 of Reference 14). Level 3 airplanes, for example, have maximum seating for between seven to nine passengers, and they have different Part 23 airworthiness requirements. One interesting configuration (while remaining a Level 4 type) is a ten-passenger variant, with a range of 379 nmi: a 51 percent increase over the design configuration. A manufacturer could offer similar variants with maximum seating varying between ten and 19 passengers to accommodate variable needs of operators. A nine-passenger variant would fall into the Level 3 classification, where a second in command is unnecessary. The weight of the second in command could be used instead as additional battery weight (as shown in Figure 13).

8.3.2 Influence of Reserves and Cruise Speed

Two other sensitivities are examined where the manner in which the airplane is flown is changed. It is of interest to determine the maximum range when energy intended for reserves is reduced from the design case, as shown in Figure 14 (left). Ordinarily, the design mission allows for 45 min of additional flying time at 180 ktas and 8000 ft. If reduced to zero, range increases to 437 nmi. This is the maximum range at full payload in the event there is a diversion to an alternate field.

The second sensitivity examined is the influence of cruise airspeed, as shown in Figure 14 (right). With 19 passengers and with 45 min of reserves, flying at 250 kcas (the maximum airspeed allowed under Part 23 for low-speed types per 14 CFR§23.2005 of Reference 14) reduces range to just 132 nmi. Higher airspeed results in a lower lift-to-drag ratio (see Figure 12).

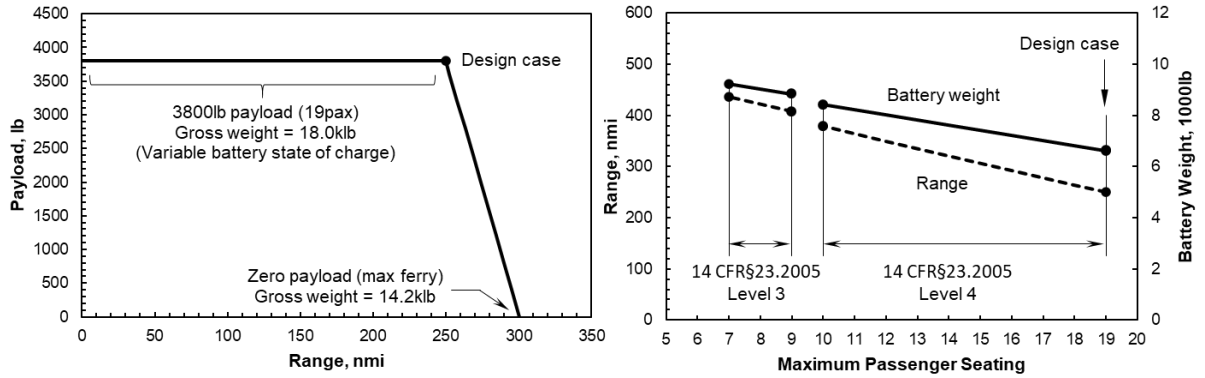

Figure 13.—Traditional payload-range diagram (left); replacing payload with batteries (right).

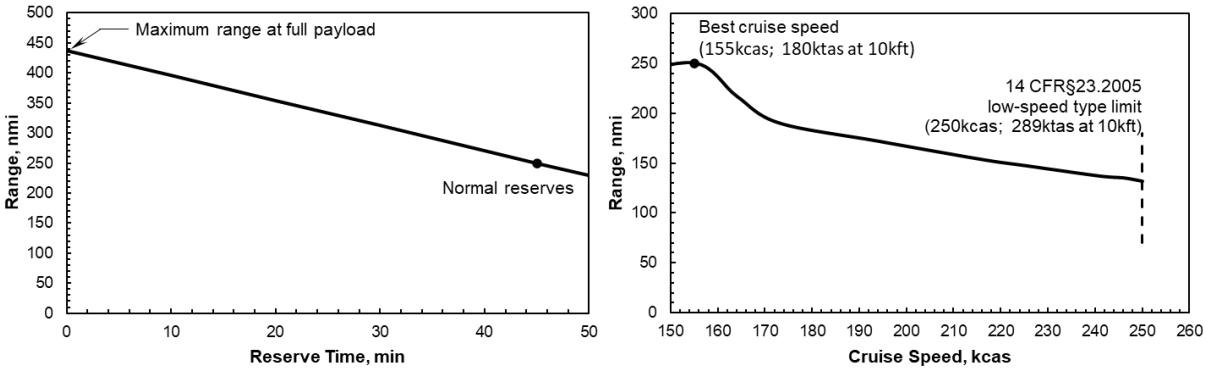

Figure 14.—Reserves sensitivity (left) and cruise speed sensitivity (right).

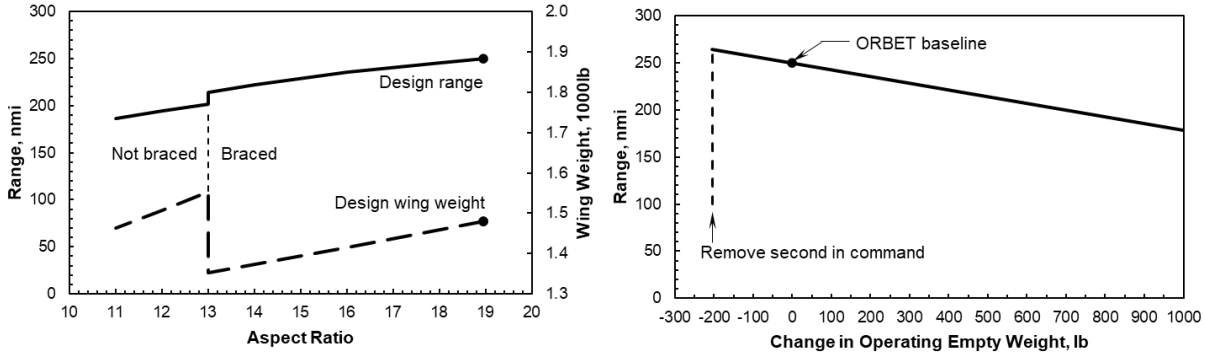

Figure 15.—Influence of aspect ratio (left) and empty weight (right).

8.3.3 Influence of Aspect Ratio and Empty Weight

The influence of aspect ratio and wing bracing is investigated. There is a significant range improvement associated with increasing aspect ratio (see Figure 15, left). Wing weight is predicted as described in Section 3.0. Wing weight increases with increasing aspect ratio, but aerodynamics and mission range improve. A brace is used for all aspect ratios greater than 13 and aspect ratio is limited to a maximum of 19. A wing brace is considered to be an enabling technology for higher aspect ratios. Weight is discontinuous when a brace is added due to the weight reduction possible with a brace.

The influence of underpredicting empty weight is also investigated to understand its resulting range penalty (see Figure 15, right). Here, mission energy is reduced as batteries are displaced by ballooning

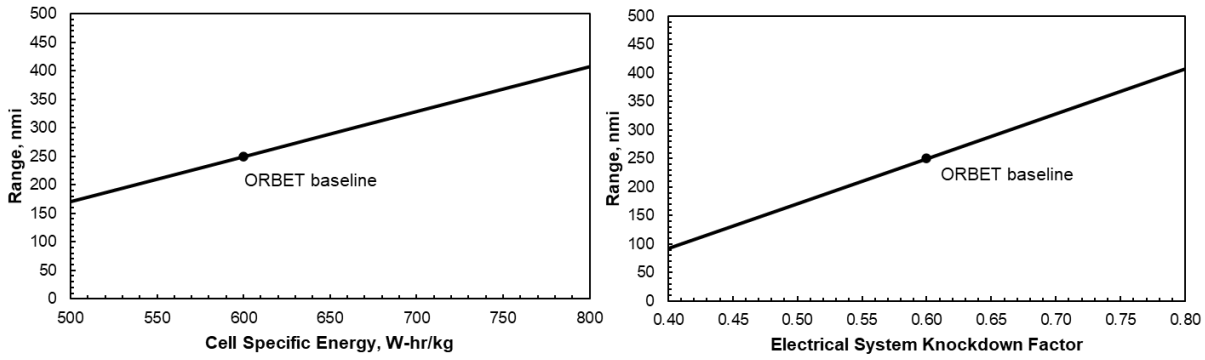

Figure 16.—Influence of specific energy (left) and electrical system knockdown factor (right).

empty weight in other categories with the 18,000 lb gross weight held constant. There is a 3 percent loss in range for every 100 lb increase in empty weight. Conversely, range can be increased if operating empty weight can be reduced. For example, if the second in command is not necessary (see the discussion in Section 3.0), then range improves by 6 percent.

8.3.4 Influence of Power System Technologies

The sensitivity of range to battery cell specific energy is investigated for values of $e_{grav,cell}$ different than the 600 W-h/kg required for the ORBET baseline (see Figure 16, left). As discussed already in Section 8.0, the cell specific energy required for the ORBET baseline is beyond the capability of current Li-ion batteries. But other battery chemistries with higher cell densities may be possible in the future.

The influence of power system technologies (discussed in Section 6.0) is also of interest. Sensitivity of range to the electrical system knockdown factor are shown in Figure 16, right.

9.0 Low-Noise Operating Mode

The noise of a propeller is a strong function of its tip speed. As a practical matter, this observation, of course, must have been made quite early on. But ordinarily, good thrust production is at odds with low tip speeds, and so designers are reluctant to build propellers that turn too slowly. Nevertheless, for airplanes equipped with variable-pitch propellers, an opportunity exists for operation at low shaft speed and maximum shaft power. At low shaft speeds, high shaft power levels and high blade pitch angles can be combined to recover much of the thrust that would otherwise be lost. This could enable a low-noise operating mode for propellers that are normally designed for performance rather than for noise. A pilot could switch between low-noise and high-performance operating modes as necessary and when practicable. Low-noise takeoffs at airports where noise is considered a problem may be possible.

Quieting propellers by means of tip speed reduction has been elusive. This has been especially true in the case of reciprocating engines, where mechanical shaft power and shaft speed are closely coupled. The maximum rated shaft power is typically produced at or near peak shaft speed. If an airplane equipped with a reciprocating engine and a variable-pitch propeller attempts a low-noise takeoff by reducing the propeller's tip speed, propeller power and thrust are reduced. Such takeoffs are not tolerated due to punishing performance effects, such as increased field lengths and poor climb rates. With a reciprocating engine, a mechanical gearbox with a variable gear ratio would be necessary to deliver peak shaft power at an arbitrary shaft speed, and it would be a means to accomplish high- and low-speed operations of a propeller. However, shifting gears (quite literally on the fly) has not become popular, despite at least one serious investigation unrelated to noise in 1941 (Ref. 92). A continuously variable transmission could

manage the job also, provided it could be made lightweight, reliable, safe, and able to handle internal forces well enough. Even given a turboshaft engine with a free power turbine (where shaft power and shaft speed can be uncoupled), modifying propellers to operate at a low tip speed to reduce noise has not become popular, perhaps because it is at odds with generating thrust efficiently or because of implementation issues.

Electric motors, and the relative ease by which their speed and power may be controlled, may be the motivating force of change. Certain electric motors are able to deliver maximum shaft power over a range of shaft speeds. Induction and synchronous electric motors, furnished with appropriate power management equipment and speed controllers, are able to vary shaft speed by adjusting the frequency of the power supplied to the motor. In application, the shaft torque can be made constant from rest to the shaft speed defined by the so-called rated frequency. But, above the rated frequency, the motor is in the field flux control, or constant voltage regime. Here, the torque diminishes with shaft speed, and the shaft output power remains relatively constant. The constant-power operating regime is the focus of this section. In practice, this behavior can be loosely described as an "electronic gearbox" that allows peak rated shaft power output to occur at a selectable range of shaft speeds. This concept is discussed for application to general aviation airplanes that ordinarily use piston engines in Reference 93.

Note this concept is not related to the *design* of a low-noise, electrically driven propeller. Indeed, that is an interesting design and optimization problem of larger scope (e.g., Ref. 94). Designing a propeller for low noise is usually at odds with generating thrust efficiently. The six-blade, wide-chord, low-speed propeller designed for the Lockheed prototype QT-2PC quiet observation plane (Ref. 95) is an example of this conflict. Instead, this study is intended to evaluate propellers *already designed for thrust and efficiency* in the low-noise mode described.

An explicit noise analysis is not performed in this study. However, takeoff reference profiles performed at reduced shaft speeds are computed. A qualitative estimate of noise reduction is given, and comments are offered on implementation in a certification setting.

9.1 Implementation as a Selectable Noise Reduction System

For takeoff and initial climbout using maximum shaft power, two operating modes are envisioned for ORBET: 1) a performance mode at a high shaft speed where thrust is maximized, and 2) a low-noise mode at a lower, selectable shaft speed. In normal operations, the mode would be chosen prior to takeoff by the flight crew, given considerations for takeoff field performance, downrange obstacles, climb rate, and, of course, community noise.

For noise certification of new, propeller-driven light airplanes such as ORBET, the provisions of Chapter 10 of the ICAO's Annex 16 (Ref. 33) apply. In a noise test for airplanes of this type, the airplane is required to take off, climb, and fly directly over a noise observation monitor on the ground, located on the extended centerline of the runway 2500 m (8202 ft) from brake release. At the noise monitoring station, a single microphone is flush-mounted over an acoustically hard surface at ground level. The two operating modes could be classified as a "selectable noise reduction system," or a SNRS, described in the ICAO Environmental Technical Manual (Ref. 96). As envisioned, an applicant would define selectable takeoff operating modes in its airplane flight manual or in its pilot's operating handbook. The regulating authority would need to approve procedures for each operating mode. The authority might certify only the noisiest of the available SNRS options for Chapter 10 compliance, but since (to date) no applicant has come forward with a SNRS, this remains to be seen. If the noisiest mode is the only mode certified, then the low-noise mode would be a means to reduce noise in operational practice only.

9.2 Takeoff Reference Profiles

If implemented as a SNRS, maximum shaft power would be constant throughout the selectable range of shaft speeds. Within this range, electric motor efficiency would of course vary. In practice, and at least without any noise considerations, the shaft speed that maximizes the combined efficiency of the electric motor, propeller system, and the entire airplane for a given flight condition and thrust requirement would be preferred. This optimization should of course be mindful of motor and propeller operating limits, and it should be an interesting engine control system challenge (Ref. 97). A full-authority digital engine control system and a clever propeller hub mechanism might be developed to schedule the propeller speed and blade pitch angle with motor system characteristics and airplane thrust requirements. Note that in this study, electric motor efficiency is not explicitly considered (it is incorporated in the electrical system knockdown factor).

Takeoff reference profiles using four shaft speeds are evaluated for noise certification under Chapter 10. Referring to Table 7, ORBET's takeoff power is 1174 bhp per motor. At this power, maximum thrust occurs at 1600 rev/min. This condition represents the takeoff performance mode setting. Reduced shaft speeds of 1300, 1200, and 1100 rev/min are considered for candidate low-noise modes. Note that absorbing large amounts of power as the shaft speed falls is not perpetually sustainable. If the shaft speed continues to fall and the blade pitch increases to compensate, eventually, the propeller blades will stall. The ORBET propeller, expected to absorb 1174 bhp at sea level static, will begin to stall at about 900 rev/min.

Certification procedures are used to compute the takeoff profiles. Following the guidance given in Reference 33, calculations are made at maximum gross weight for a sea level runway at 59 °F and zero wind using FLOPS software (Ref. 34). At brake release, maximum power is applied and flaps are deployed at their takeoff setting. Once aloft, the landing gear is retracted and the airplane changes to its climb configuration at a point determined by the applicant. In the climb configuration, flaps may be repositioned, and airspeed must be maintained at a speed that maximizes the rate of climb. In the case of ORBET, maximum climb rate over the noise monitor occurs when flaps are retracted at 200 ft and when the climbout speed is held at 122 kcas. Takeoff reference profiles using the four shaft speeds are shown in Figure 17.

Procedures from Section 10.5.2 of Reference 33 require engine "takeoff power" to be selected and maintained throughout the noise test to a point beyond the noise measurement location. But takeoff power may seem a bit hazily defined when discussing airplanes having electrical power, especially when (as in this study) maximum mechanical shaft power can occur over a selectable range of shaft speeds. To put it another way, maximum power does not necessarily coincide with maximum thrust. In the case of light aircraft powered by reciprocating engines or small turbine engines, the intent of the regulation is to require airplanes to operate at their maximum takeoff-rated engine power as defined in the Airplane Flight Manual or the Pilot's Operating Handbook. In the case of a small electric airplane, it is possible that a manufacturer could list more than one engine "takeoff power" rating in its manual. Hypothetically, two takeoff ratings could be defined for ORBET: both would use maximum shaft power, but they would have different shaft speeds. For a short field and best climb performance, the propeller would be set for maximum thrust at 1600 rev/min. For a quieter takeoff, a second takeoff setting could be defined at a lower propeller speed.

The 1300 rev/min takeoff profile seems to be an attractive candidate for the low-noise mode. Relative to the performance mode, field distance to the 35 ft runway obstacle increases by only 9 percent, and climb rate decreases by only 4 percent. But tip speed is 19 percent lower relative to the performance mode. If propeller noise varies (roughly) by tip speed to the fifth power, this would result in a generalized source noise reduction of 4 to 5 dB. For a receiver at ground level, this noise benefit would be eroded by about 0.7 dB due to the altitude loss (see Figure 17, top). A more detailed study of takeoff performance and noise is needed.

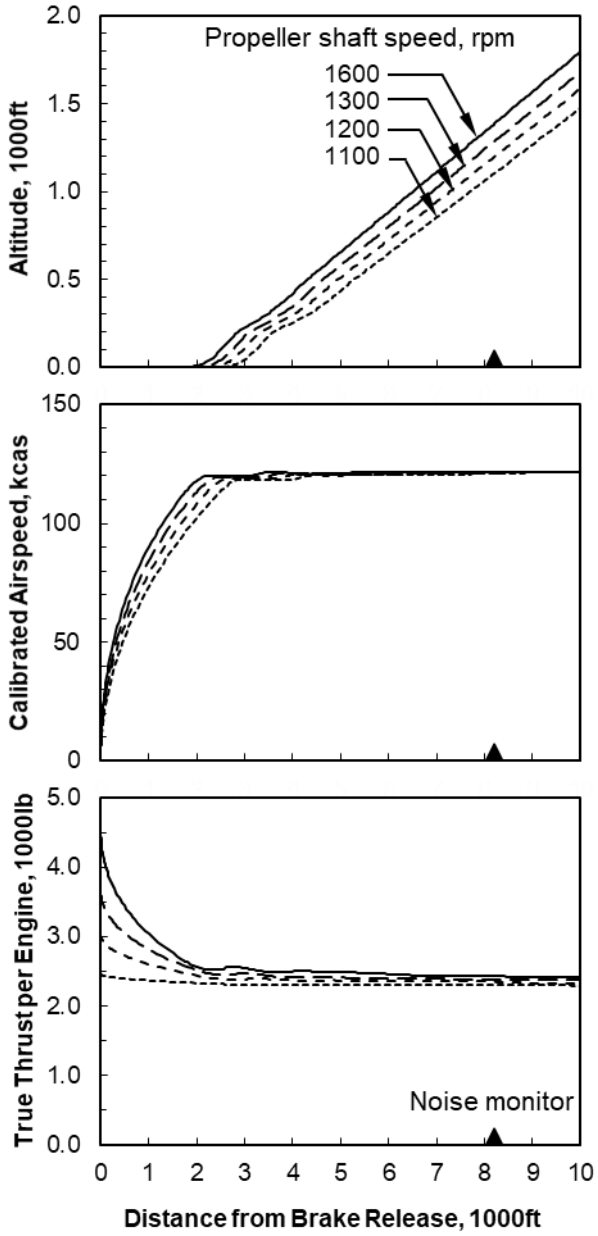

Figure 17.—Influence of shaft speed on takeoff reference profile.

10.0 Summary

A notional, 19-passenger, fully electric transport with a braced wing and two propellers is investigated. Parametric system weight, aerodynamic, propeller, and mission performance models are developed to aid sizing and optimization. Battery cell specific energy is treated as a technology parameter that is varied to determine its influence on mission range. To achieve a minimum range success criterion of 250 nmi with 45 min of reserve power, it is found that battery cell specific energy must be at least 600 W-h/kg, more than twice the capability of today's lithium-ion cells. Success of the ORBET design is dependent on progress in battery technology.

Single-rotation and contra-rotation propellers are studied. The contra-rotation propellers are not found to improve performance. Swirl losses introduced by the front propeller may not be great enough to justify a contra-rotating aft propeller. Implementation of a novel selective noise reduction system is proposed.

This study is intended to broadly define a relatively near-term, fully electric, 19-passenger airplane. It was conducted as a part-time effort lasting just nine months. Due to the short time involved, this study does not assess the concept's marketability, its operating costs, or the additional airport infrastructure required to support it. Future work is needed to model the concept and its economics more rigorously.

11.0 Future Work

This study would benefit from refined analyses in all of its disciplines. One possibility is to place it within research focused on the Transonic Truss Braced Wing concept (Ref. 13). NASA, FAA, industry and academia are studying the TTBW through the Sustainable Flight National Partnership (Ref. 12). Though ORBET is much smaller and cruises at speeds considerably slower than the TTBW, their braced wings are architecturally similar. ORBET could serve as another vehicle concept under those studies. A smaller vehicle could act as an additional challenge to the tools under development in NASA's model-based systems analysis initiative (Ref. 98).

References

1. Conner, M. (ed.): "NASA Armstrong Fact Sheet: NASA X-57 Maxwell," NASA X-57 Fact Sheet, Sept. 2018 [URL: https://www.nasa.gov/centers/armstrong/news/FactSheets/FS-109.html, accessed Aug. 2022].
2. Gipson, L. (ed.): "Hybrid Wing Body Goes Hybrid," NASA N3-X Fact Sheet, Feb. 2013 [URL: https://www.nasa.gov/content/hybrid-wing-body-goes-hybrid/, accessed Aug. 2022].
3. Dambowsky, F. (ed.): "Hybrid-Electric Propulsion Systems Enable more Climate-Friendly Air Transport," DLR Regional Aircraft Fact Sheet, Nov. 2021 [URL: https://www.dlr.de/content/en/articles/news/2021/04/ 20211122_hybrid-electric-propulsion-enable-more-climate-friendly-air-transport.html/, accessed Aug. 2022].
4. Jaggi, R.: "This Radical New eVTOL Uses 30 Tilting 'Jet' Fans to Get in the Air and Stay There," Lilium eVTOL, Robb Report, Aug. 2022 [URL: https://robbreport.com/motors/aviation/30-jet-evtol-tested-spain-will-it-work-1234739016/, accessed Aug. 2022].
5. Stückl, S.; van Toor, J.; and Lobentanzer, H.: "VOLTAIR - The All Electric Propulsion Concept Platform - A Vision for Atmospheric Friendly Flight," In Proceedings of the 28th International Congress of the Aeronautical Sciences, Brisbane, Australia, pp. 1–11, 2012.
6. Antcliff, K.; Guynn, M.; Marien, T.; Wells, D.; Schneider, S.; and Tong, M.: "Mission Analysis and Aircraft Sizing of a Hybrid-Electric Regional Aircraft," AIAA paper 2016-1028, 2016.
7. Marien, T.; Blaesser, N.; Frederick, Z.; Guynn, M.; Kirk, J.; Fisher, K.; Schneider, S.; Thacker, R., and Frederic, P.: "Results for an Electrified Aircraft Propulsion Design Exploration," AIAA paper 2021-3280, 2021.
8. Pornet, C.; Gologan, C.; Vratny, P.C.; Seitz, A.; Schmitz, O.; Isikveren, A.; and Hornung, M.: "Methodology for Sizing and Performance Assessment of Hybrid Energy Aircraft," *J. Aircraft*, vol. 52, no. 1, pp. 341-52, 2014.
9. Hoelzen, J.; Liu, Y.; Bensmann, B.; Winnefeld, C.; Elham, A.; Friedrichs, J.; and Hanke-Rauschenbach, R.: "Conceptual Design of Operation Strategies for Hybrid Electric Aircraft," *MDPI Energies* vol. 11, no. 1, 217, 2018.

10. Mukhopadhaya, J.; and Rutherford, D.: “Performance analysis of evolutionary hydrogen-powered aircraft,” ICCT white paper, 2022 [URL: https://theicct.org/wp-content/uploads/2022/07/global-aviation-performance-analysis-regional-electric-aircraft-jul22-1.pdf-1.pdf, accessed Aug. 2022].
11. Kuhn, H.; Seitz, A.; Lorenz, L.; Isikveren, A.; and Sizmann, A.: “Progress and Perspectives of Electric Air Transport,” Proceedings of the 28th Congress of the International Council of the Aeronautical Sciences ICAS, Brisbane, Australia, vol. 6, pp. 4886-4899, 2012.
12. Gipson, L. (ed): “Sustainable Flight National Partnership,” NASA press release, Feb. 2022 [URL: https://www.nasa.gov/aeroresearch/sustainable-aviation-np/, accessed Aug. 2022].
13. Smith, Y. (ed): “Trans-Sonic Truss-Braced Wing May Help Reduce Fuel Consumption,” NASA press release, Sept. 2021 [URL: https://www.nasa.gov/image-feature/trans-sonic-truss-braced-wing-may-help-reduce-fuel-consumption, accessed Aug. 2022].
14. U.S. Code of Federal Regulations, Title 14, Chap. I, Part 23, “Airworthiness Standards: Normal Category Airplanes.”
15. European Aviation Safety Agency: “Certification Specifications for Normal, Utility, Aerobatic and Commuter Category Aeroplanes”, CS-23 Initial Issue, 2003.
16. Greitzer, E., et al.: “N+3 Aircraft Concept Designs and Trade Studies, Final Report, Volume 1,” NASA/CR-2010-216794, 2010.
17. Department of Transportation and National Aeronautics and Space Administration: “Civil Aviation Research and Development Policy Study,” DOT TST-10-4, NASA SP-265, 1971.
18. Johnson, W.; and Silva, C.: “NASA Concept Vehicles and the Engineering of Advanced Air Mobility Aircraft,” *The Aeronautical Journal*, vol. 126, no. 1295, pp. 59-91, 2022.
19. Harish, A.; Perron, C.; Bavaro, D.; Ahuja, J.; Ozcan, M.; Justin, C.; Briceno, S.; German, B.; and Mavris, D.: “Economics of Advanced Thin-Haul Concepts and Operations,” AIAA paper 2016-3767, 2016.
20. U.S. Department of Transportation: “Essential Air Service,” [URL: https://www.transportation.gov/policy/aviation-policy/small-community-rural-air-service/essential-air-service, accessed Sept. 2022].
21. Federal Aviation Administration: “Textron Aviation, Inc., Model 408 Type Certificate Data Sheet,” TCDS no. A00016WI, rev. 0, March 2022.
22. Federal Aviation Administration: “Airport Data and Information Portal,” Advanced Facility Search, [URL: https://adip.faa.gov/agis/public/#/airportSearch/advanced, accessed Sept. 2022].
23. Schuh, G.; Spangenberg, M.; Zhang, Q.; Dannbeck, B.; and Stuerken, J.: “Economic Feasibility Study of a Hybrid-Electric 19-Passenger Commuter Aircraft,” Deutscher Luft- und Raumfahrtkongress, doc. ID 530307, 2021.
24. Spangenberg, M: “D2.1 Economic Feasibility Study for a 19 PAX Hybrid-Electric Commuter Aircraft,” Economic Feasibility Study, Clean Sky 2 Grant no. 864551, 2020 [URL: https://www.rolls-royce.com/~/media/Files/R/Rolls-Royce/documents/innovation/elicad2-1-economic-feasibility-study-for-a-19-pax-hybrid-electric-commuter-aircraft.pdf, accessed Sept. 2022).
25. Textron Aviation, Inc.: “Cessna SkyCourier: Specification and Description, Serial Number 408-0003 to TBD,” SD-TBP-C408-0622, June 2022.
26. Wolf, D.: “Commuter Airline Perspective,” Joint NASA-FAA On-Demand Mobility and Emerging Technology Workshop, Arlington, VA, March, 2016.
27. Jansen, R.; Bowman, C.; Clarke, S.; Avanesian, D.; Dempsey, P.; and Dyson, R.: “NASA Electrified Aircraft Propulsion Efforts,” NASA report no. GRC-E-DAA-TN72947, NATO report no. STO-MP-AVT-323, 2019.

28. Aultman-Hall, L.; Harvey, C.; Sullivan, J.; and LaMondia, J: "The Implications of Long-Distance Tour Attributes for National Travel Data Collection in the United States," *Transportation*, vol. 45, pp. 875-903,2018.
29. National Academies of Sciences, Engineering, and Medicine: "Interregional Travel: A New Perspective for Policy Making," The National Academies Press, Washington, DC, 2016.
30. European Commission, Directorate-General for Mobility and Transport, Directorate-General for Research and Innovation: "Flightpath 2050: Europe's Vision for Aviation, Maintaining Global Leadership and Serving Society's Needs," Publications Office, 2011 [URL: https://data.europa.eu/doi/10.2777/50266, accessed Sept. 2022].
31. U.S. Code of Federal Regulations, Title 14, Chap. I, Part 91, "General Operating and Flight Rules."
32. Schuh, G.; Spangenberg, M.; and Zhang, Q.: "Economically Driven Requirements for a Hybrid-Electric 19-Passenger Commuter Aircraft," IOP Conference Series: Material Science and Engineering, 1024, 012079, 2021.
33. "Annex 16 to the Convention on International Civil Aviation Environmental Protection," Vol. I, Aircraft Noise," International Standards and Recommended Practices—Environmental Protection, 7th ed., International Civil Aviation Org., Montreal, July 2014.
34. McCullers, L.A.: "Aircraft Configuration Optimization Including Optimized Flight Profiles, Multidisciplinary Analysis and Optimization Part 1," NASA CP-2327, pp. 396-412, 1984.
35. European Aviation Safety Agency: "Dornier 228 Series Type Certificate Data Sheet," TCDS no. EASA.A.359, issue 07, Dec. 2021.
36. European Aviation Safety Agency: "PZL M28 Type Certificate Data Sheet," TCDS no. EASA.A.058, issue 08, Nov. 2015.
37. Federal Aviation Administration: "Viking Air Limited, DHC-6 Twin Otter Type Certificate Data Sheet," TCDS no. A9EA, rev. 21, Feb. 2018.
38. Khan, K.; Mallik, W.; Kapania, R.; and Schetz, J.: "Distributed Design Optimization of Large Aspect Ratio Wing Aircraft with Rapid Transonic Flutter Analysis in Linux," AIAA paper 2021-1354, 2021.
39. Chakraborty, I.; Nam, T.; Gross, J.; and Mavris, D.: "Comparative Assessment of Strut-Braced and Truss-Braced Wing Configurations Using Multidisciplinary Design Optimization," *J. of Aircraft*, vol. 52, no. 6, 2015.
40. Nguyen, N.; and Xiong, J.: "CFD-Based Frequency Domain Method for Dynamic Stability Derivative Estimation with Application to Transonic Truss-Braced Wing." AIAA paper 2022-3596, 2022.
41. Demasi, L.; Monegato, G; Cavallaro, R.; and Rybarczyk, R.: "Minimum Induced Drag Conditions for Truss-Braced Wings," *AIAA Journal*, vol. 56, no. 12, 2018.
42. Duggirala, R.; Roy, C.; and Schetz, J: "Analysis of Interference Drag for Strut–Strut Interaction in Transonic Flow," *AIAA Journal*, vol. 49, no. 3, 2021.
43. Secco, N.; and Martins, J.: "RANS-Based Aerodynamic Shape Optimization of a Strut-Braced Wing with Overset Meshes," *J. of Aircraft*, vol. 56, no. 1, 2019.
44. Wells, D.P.; Horvath, B.L.; and McCullers, L.A.: "The Flight Optimization System Weights Estimation Method," NASA-TM-2017-219627, Volume I, 2017.
45. Hager, R.; and Vrabel, D.: "Advanced Turboprop Project," NASA SP-495, 1988.
46. Trimble, S.: "Quiet Revolution: Open-rotor engines promise a new era of fuel efficiency but their inherently high noise has ruled them out – until now," Flight International, 25 Feb.-3 Mar, 2014.
47. U.S. Code of Federal Regulations, Title 14, Chap. I, Part 25, "Airworthiness Standards: Transport Category Airplanes."

48. U.S. Department of Transportation: “Minimizing the Hazards from Propeller Blade and Hub Failures,” Federal Aviation Administration, Advisory Circular, AC 25.905-1, 2000.
49. U.S. Code of Federal Regulations, Title 14, Chap. I, Part 35, “Airworthiness Standards: Propellers.”
50. Torenbeek, E.: “Synthesis of Subsonic Airplane Design,” ISBN 90-247-2724-3, Delft University Press, Delft, Netherlands, 1982 (reprinted 1996).
51. McCullers, L.A.; and Lynch, R.W.: “Dynamic Characteristics of Advanced Filamentary Composite Structures, Volume II - Aeroelastic Synthesis Procedure Development,” AFFDL-TR-73-111, 1974.
52. McCullers, L.A.: “Flight Optimization System User’s Manual, Version 8.29,” maintained and released by NASA.
53. National Aeronautics and Space Administration: “NASA Spinoff: Deicing System Protects General Aviation Aircraft,” NASA/NP-2007-10-484-HQ, 2007.
54. Roland, H.: “Advance Design Weight Analysis and Systems and Equipment Weight Prediction,” Society of Allied Weight Engineers paper no. 790, 28th Annual Conference, San Francisco, California, May 5-8, 1969.
55. Hinetics, LLC.: “Integrated High Frequency Electric Propulsor for Turbo-Electric Aircraft,” SBIR 18-1-A1.07-8322, contract 80NSSC18P1898, 2019 (URL: https://www.sbir.gov/sbirsearch/detail/1559639, accessed July 2022).
56. Zhang, X.; Bowman, C.; O’Connell, T.; and Haran, K.: “Large Electric Machines for Aircraft Electric Propulsion,” *IET Electr. Power Appl*., vol. 12, no. 6, 2018, pp. 767-779.
57. U.S. Code of Federal Regulations, Title 14, Chap. I, Part 135, “Operating requirements: Commuter and on-demand operations and rules governing persons on board such aircraft.”
58. Roskam, J.: “Airplane Design, Part VI: Preliminary Calculation of Aerodynamic, Thrust and Power Characteristics,” Roskam Aviation and Engineering Corporation, Kansas, 1990.
59. Hunter, J.: “Jane’s Aircraft Upgrades, 2009-2010”, Jane's Information Group, 2010.
60. Sadraey, M.: “Aircraft Design: A Systems Engineering Approach (Chap. 5, Wing Design),” Print ISBN 9781119953401, John Wiley & Sons, Ltd., 2012.
61. Drela, M.: “XFOIL: An Analysis and Design System for Low Reynolds Number Airfoils,” In *Low Reynolds Number Aerodynamics, Lecture Notes in Engineering*, vol. 54, Springer, Berlin, Heidelberg, 1989.
62. Joslin, R.: “Overview of Laminar Flow Control,” NASA/TP-1998-208705, 1998.
63. Drela, M.; and Youngren, H: “XROTOR website,” (URL: https://web.mit.edu/drela/Public/web/xrotor/, accessed Aug. 2022).
64. Betz, A. (with an appendix by Ludwig Prandtl): “Schraubenpropeller mit geringstem Energieverlust (Screw Propellers with Minimum Energy Loss), Goettingen Reports, 1919.
65. Wainauski, H.; and Simsbury, C.: “Airfoil Blade,” United States Patent no. 4,519,746, United Technologies Corp., 1985.
66. Black, D.; Magliozzi, B.; and Rohrbach, C.: “Small Transport Aircraft Technology Propeller Study,” NASA CR-168 (045), 1983.
67. Chapman, J.; Schnulo, S.; and Nitzsche, M.: “Development of a Thermal Management System for Electrified Aircraft,” AIAA paper 2020-0545, 2020.
68. National Academy of Science, Engineering, and Medicine, “Commercial Aircraft Propulsion and Energy Systems Research: Reducing Global Carbon Emissions,” Committee on Propulsion and Energy Systems to Reduce Commercial Aviation Carbon Emissions, Aeronautics and Space Engineering Board Division on Engineering and Physical Sciences, The National Academies Press, Washington D.C., 2016.

69. Löbberding, H.; Wessel, S.; Offermanns, C.; Kehrer, M.; Rother, J.; Heimes, H.; Kampker, A.: "From Cell to Battery System in BEVs: Analysis of System Packing Efficiency and Cell Types," *MDPI World Electr. Veh. J.*, vol. 11, no. 4, 2022.
70. Schnulo, S.; Hall, D.; Chin, J.; and Smith, A.: "Further Development of the NASA X-57 Maxwell Mission Planning Tool for Mods II, III, and IV," AIAA paper 2019-4491, 2019.
71. Gray, J., Moore, K., Hearn, T., and Naylor, B., "Standard Platform for Benchmarking Multidisciplinary Design Analysis and Optimization Architectures," *AIAA Journal*, vol. 51, no. 10, Oct. 2013, pp. 2380–2394; also AIAA Paper 2012-1586, April 2012.
72. Gray, J.; Hwang, J.; Martins, J.; Moore, K.; and Naylor, B.: "OpenMDAO: an open-source framework for multidisciplinary design, analysis, and optimization," *Struct. Multidisc. Optim.*, vol. 59, 2019, pp. 1075-1104 (doi 10.1007/s00158-019-02211-z).
73. Jansen, P.W.; and Perez, R.E.: "Constrained Structural Design Optimization via a Parallel Augmented Lagrangian Particle Swarm Optimization Approach," *Comput. Struct.*, vol. 89, no. 13, 2011, pp. 1352-1366.
74. Kraft, D.: "A Software Package for Sequential Quadratic Programming," Tech. Rep. DFVLR-FB 88-28, DLR German Aerospace Center, Institute for Flight Mechanics, Koln, Germany, 1988.
75. Conlon, B.; et al., "The Next Generation 'Voltec' Extended Range EV Propulsion System," *SAE Int. J. Alt. Power*, vol. 4, no. 2, pp. 248-259, 2015.
76. Xiong, J.; Fugate, J.; and Nguyen, N.: "Investigation of Truss-Braced Wing Aircraft Transonic Wing-Strut Interference Effects Using FUN3D," AIAA Paper 2019-3026, 2019.
77. June, J.; Thomas, R.; and Guo, Y.: "System Noise Technology Roadmaps for a Transonic Truss-Braced Wing and Peer Conventional Configuration," AIAA Paper 2022-3049, 2022.
78. Lambe, A.; and Martins, J.: "Extensions to the design structure matrix for the description of multidisciplinary design, analysis, and optimization processes," *Struct. Multidisc. Optim.*, vol. 46, 2012, pp. 273-284 (doi 10.1007/s00158-012-0763-y).
79. Borst, H., "Summary of Propeller Design Procedures and Data, Volume 1: Aerodynamic Design and Installation," U.S. Army Air Mobility Research and Development Laboratory, accession no. AD-774-831, 1973.
80. Gur, O.; and Rosen, A.: "Optimization of Propeller Based Propulsion System," *J. of Aircraft*, vol. 46, no. 1, January–February 2009.
81. Karabelli, D.; and Birke, K.P.: "Feasible Energy Density Pushes of Li-Metal vs. Li-Ion Cells," *MDPI Appl. Sci.*, vol. 11, no. 16, 2021.
82. Liu, Y.; Liu, S.; Li, G.; and Gao, X.: "Strategy of Enhancing the Volumetric Energy Density for Lithium–Sulfur Batteries," *Adv. Materials* (Weinheim), vol. 33, no. 8, p. 2003955, 2021.
83. Xue, W.; Miao, L.; Qie, L.; Wang, C.; Li, S.; Wang, J.; and Li, J.: "Gravimetric and Volumetric Energy Densities of Lithium-Sulfur Batteries," *Current Opinion in Electrochemistry*, vol. 6, no. 1, pp. 92-99, 2017.
84. McCloskey B D: "Attainable Gravimetric and Volumetric Energy Density of Li-S and Li Ion Battery Cells with Solid Separator-Protected Li Metal Anodes," *J. Phys. Chem. Lett.*, vol. 6: pp. 4581-4588, 2015.
85. Hagen, M.; Hanselmann, D.; Ahlbrecht, K.; Maça, R.; Gerber, D.' and Tübke, J.: "Lithium–Sulfur Cells: The Gap between the State-of-the-Art and the Requirements for High Energy Battery Cells," *Adv. Energy Mater.*, vol. 5, no. 16, p. 1401986, 2015.
86. Hubbard, H.: "Sound from Dual-Rotating and Multiple Single-Rotating Propellers," NACA TN 1654, 1948.

87. Block, P.: “Noise Radiation Patterns of Counter-Rotation and Unsteadily Loaded Single-Rotation Propellers,” *J. Aircraft*, vol. 22, no. 9, pp. 776-783, 2012.
88. Tam, C.; Salikuddin, M.; and Hanson, D.: “Acoustic Interference of Counter-Rotation Propellers, *J. Sound & Vibr.*, vol. 124, no. 2, pp. 357-366, 1988.
89. Smith, D.; Filippone, A.; and Bojdo, N.: “Noise reduction of a Counter Rotating Open Rotor through a locked blade row,” *Aerospace Science and Technology*, vol. 98, 2020.
90. Guynn, M.; Berton, J.; Haller, W.; Hendricks, E.; and Tong, M.: “Performance and Environmental Assessment of an Advanced Aircraft with Open Rotor Propulsion,” NASA TM 2012-217772, 2012.
91. Strack, W.; Knip, G.; Weisbrich, A.; Godston, J.; and Bradley, E.: “Technology and Benefits of Aircraft Counter Rotation Propellers,” NASA TM 82983, 1982.
92. Pankhurst, R. C.; Conn, J. F. C.; Fowler, R. G.; and Love, E. M.: “The Effect of Variation of Gear Ratio on the Performance of a Variable-Pitch Airscrew for a High-Speed Aeroplane,” Ministry of Aircraft Production, Aeronautical Research Committee R&M 2039, London, Oct. 1941.
93. Berton, J.; and Nark, D.: “Low-Noise Operating Mode for Propeller-Driven Electric Airplanes,” *J. of Aircraft*, vol. 56, no. 4, pp. 1708-1714. 2019.
94. Gur, O.; and Rosen, A.: “Design of a Quiet Propeller for an Electric Mini Unmanned Air Vehicle,” *J. of Propulsion and Power*, vol. 25, no. 3, pp. 717-728, May-June 2009.
95. Francillon, René J.: “Lockheed Aircraft Since 1913,” London, Putnam & Co., 1982, ISBN 0-370-30329-6.
96. “Environmental Technical Manual, Vol. I, Procedures for the Noise Certification of Aircraft,” International Civil Aviation Organization (ICAO), Committee on Aviation Environmental Protection, 2nd ed., Document 9501, 2015, pp. 3.47-3.48.
97. McDonald, R.: “Modeling of Electric Motor Driven Variable Pitch Propellers for Conceptual Aircraft Design,” AIAA Paper 2016-1025, Jan. 2016.
98. Clarke, J.: “NASA Advisory Council Meeting - Aeronautics Report,” National Advisory Council Committee report, Aug. 2022 [URL: https://www.nasa.gov/sites/default/files/atoms/files/nac_aeronautics_committee_report_august_2022.pdf, accessed Sept. 2022].